Available online at www.sciencedirect.com
ScienceDirect
Geochimica et Cosmochimica Acta 72 (2008) 5757–5780
Geochimica et Cosmochimica Acta
www.elsevier.com/locate/gca

The LaPaz Icefield 04840 meteorite: Mineralogy, metamorphism, and origin of an amphibole- and biotite-bearing R chondrite

M.C. McCanta [a,*,1], A.H. Treiman [a], M.D. Dyar [b], C.M.O'D. Alexander [c], D. Rumble III [d], E.J. Essene [e]

[a] Lunar and Planetary Institute, 3600 Bay Area Boulevard, Houston, TX 77058, USA
[b] Department of Astronomy, Mount Holyoke College, South Hadley, MA 01075, USA
[c] Department of Terrestrial Magnetism, Carnegie Institution of Washington, 5241 Broad Branch Road, NW, Washington, DC 20015-1305, USA
[d] Geophysical Laboratory, Carnegie Institution of Washington, 5251 Broad Branch Road, NW, Washington, DC, 20015-1305, USA
[e] Department of Geological Sciences, University of Michigan, 2534 CC Little Building, 1100 North University Avenue, Ann Arbor, MI 48109-1005, USA

Received 7 February 2008; accepted in revised form 25 July 2008; available online 11 September 2008

Abstract

The R chondrite meteorite LaPaz Icefield (LAP) 04840 is unique among metamorphosed, non-carbonaceous chondrites in containing abundant OH-bearing silicate minerals: ~13% ferri-magnesiohornblende and ~0.4% phlogopite by volume. Other minerals include olivine (Fo_{62}), orthopyroxene ($En_{69}Fs_{30}Wo_1$), albite ($An_8Ab_{90}Or_2$), magnetite, pyrrhotite, pentlandite, and apatite. Ferromagnesian minerals are rich in Fe^{3+}, as determined by Mössbauer spectrometry and electron microprobe chemical analyses. Fe^{3+}/Fe_{tot} values are olivine $\leqslant$5%, amphibole 80%, phlogopite 65%, and magnetite 42%. Mineral compositions are nearly constant across grains and the section, except for a small variability in amphibole compositions reflecting the edenite exchange couple ($^{A}Na + {}^{IV}Al \leftrightarrow {}^{A}\square + Si$). These mineral compositions, the absence of Fe–Ni metal, and the oxygen isotope data support its classification as an R (Rumuruti) chondrite. LAP 04840 is classified as petrologic grade 5, based on the chemical homogeneity of its minerals, and the presence of distinctly marked chondrules and chondrule fragments in a fine-grained crystalline matrix. The mineral assemblage of LAP 04840 allows calculation of physical and chemical conditions at the peak of its metamorphism: $T = 670 \pm 60$ °C from a amphibole–plagioclase thermometer; P_{H_2O} between 250 and 500 bars as constrained by the assemblage phlogopite + orthopyroxene + olivine + feldspar and the absence of diopside; P_{CO_2} unconstrained; f_{O_2} at QFM + 0.5 log units; $\log(f_{HF}/f_{H_2O}) \approx -5.8$; $\log(f_{HCl}/f_{H_2O}) \approx -3.3$; and $\log(f_{HCl}/f_{HF}) \approx -2.6$. The hydrogen in LAP 04840 is very heavy, an average δD value of $+3660 \pm 75$‰ in the magnesiohornblende. Only a few known sources of hydrogen have such high δD and are suitable sources for LAP 04840: ordinary chondrite phyllosilicates (as in the Semarkona chondrite), and insoluble organic matter (IOM) in ordinary chondrites and CR chondrites. Hydrogen from the IOM could have been released by oxidation, and then reacted with an anhydrous R chondrite (at high temperature), but it is not clear whether this scenario is correct.

1. INTRODUCTION

The distribution and origin of water in the solar system is a major issue in the planetary sciences because of water's importance in the origin and sustenance of life, its influences on planetary evolution and tectonics, and its use in human exploration. Thus, NASA's exploration strategy (at least for Mars) is one of "follow the water". Therefore,

* Corresponding author.
E-mail addresses: mmccanta@caltech.edu, molly.mccanta@gmail.com (M.C. McCanta).
[1] Present address: Division of Geological and Planetary Sciences, California Institute of Technology, MS 170-25 Pasadena, CA 91125, USA.

0016-7037/$ - see front matter © 2008 Elsevier Ltd. All rights reserved.
doi:10.1016/j.gca.2008.07.034

the discovery of new water-bearing solar system material is significant, and here we report such a find: the meteorite LAP 04840, a Rumuruti (R) group chondrite, with abundant OH-bearing silicate minerals.

The LAP 04840 meteorite is the first non-carbonaceous chondritic object with abundant 'water', more precisely with abundant hydroxyl in its minerals. Hydrogen-rich materials (including clays and hydrocarbons) are present and abundant in carbonaceous materials of the early solar system, including many types of asteroids (B, C, D, F, and G classes; e.g., Vilas and Gaffey, 1989; Vilas et al., 1993, 1994), many carbonaceous chondrite meteorites (e.g., Bischoff, 1998a; Brearley and Jones, 1998), comets (Mumma et al., 1993; Davies et al., 1997), and many interplanetary dust particles (e.g., Tomeoka and Busek, 1985). Many moons of the giant planets contain abundant water and/or ice, like Europa (e.g., Greeley et al., 1998) and Enceladus (Porco et al., 2006) and phases of H_2O occur throughout the rocky bodies of the solar system, including Earth, Mars, Moon, the asteroid belt, and the moons of the outer planets. Mars has abundant water as ground ice and ice caps (Carr, 1996; Malin and Edgett, 2000; Boynton et al., 2002; Feldman et al., 2002; Christensen et al., 2004; Bibring and the OMEGA team, 2006; Squyres et al., 2006), had chemically active groundwater (Treiman, 2005), and some of its magmas may have contained percent levels of H_2O (Lentz et al., 2001, but see Treiman et al., 2006). Venus probably once had much more water and even possibly an ocean (e.g., Donahue et al., 1982), and Mercury may have water ices at its poles (Slade et al., 1992). Even the Moon, long considered to be completely dry, is not free of hydrogen. Hydrogen implanted in the lunar regolith by solar wind (Heiken et al., 1991), and it is relatively abundant in polar regions (Feldman et al., 1998, 2000). And now some lunar magmas, once considered devoid of H-bearing components, have recently been shown to contain tens of ppm of H, and may have contained hundreds of ppm H before eruption (Saal et al., 2007).

To this panoply of solar system hydrogen reservoirs, one can add the LaPaz Icefield (LAP) 04840 meteorite, found in Antarctica by the 2003–2004 ANSMET expedition (Satterwhite and Righter, 2006). LAP 04840 is a fusion-crusted stone with a dark green interior; it originally weighed 50.4 g. Preliminary examination showed it to be a non-carbonaceous chondrite, with abundant well-defined chondrules. Its oxygen isotopic composition is in the range of the R chondrites, and it is distinct from those of other non-carbonaceous chondrite groups (Bischoff et al., 1994; Rubin and Kallemeyn, 1994; Schulze et al., 1994; Kallemeyn et al., 1996). Other features support classification of LAP 04840 as an R chondrite: the magnesium number (Mg#) of its silicate minerals, its relatively high oxidation state compared to other meteorite classes (evidenced by the absence of Fe–Ni metal, and significant abundances of ferric iron in its silicate and oxide minerals), and a low chondrule/matrix ratio (Bischoff et al., 1994; Rubin and Kallemeyn, 1994; Schulze et al., 1994; Kallemeyn et al., 1996; Bischoff, 2000). LAP 04840 is unique among R chondrites in that it contains ca. 13% of OH-rich ferri-magnesiohornblende as well as a small proportion of OH-rich ferrian phlogopite (0.4%, Table 1). Other R chondrites and other non-carbonaceous chondrites are nearly dry and lack H-bearing minerals, making LAP 04840 truly unique among metamorphosed meteorites.

Here, we provide basic petrographic and mineralogic data on LAP 04840 as a basis for a better understanding of the origins of its hydrous minerals and the origin of their hydrogen. Chemical analyses and X-ray maps by electron microprobe are augmented by secondary ion probe analyses of H and other volatile elements and hydrogen/deuterium ratios and oxygen isotope measurements. The conditions of metamorphism for LAP 04840 (pressure, temperature, water pressure, and oxidation state) are then derived from mineral compositions. Finally, we attempt to interpret the hydrogen/deuterium ratio in terms of known reservoirs and suggest a possible origin for this unique hydrous chondrite.

Table 1
Mineral proportions in LAP 04840 and selected other R chondrites

Mineral	Area (%)			Rumuruti	Acfer 217	ALH 85151	Carlisle lakes	PCA 91002
	Region 1	Region 2	Average					
Olivine	60.7	65.2	63.0	70.4	72.5	53.1	55.9	65.3
Low-Ca pyroxene	13.8	3.0	8.4	0.5	2.8	13.3	9.1	8.5
Ca-pyroxene	n.d.[a]	n.d.	n.d.	5.2	4.0	11.9	9.8	6.5
Magnesiohornblende	12.1	14.8	13.4	n.d.	n.d.	n.d.	n.d.	n.d.
Feldspar	7.6	6.9	7.2	14.5	7.3	16.2	16.1	11.3
Opaques	5.6	8.7	7.2	8.9	1.9	4.6	8.5	7.9
Oxides	2.1	3.0	2.6	0.9	1.7	0.1	0.3	0.7
Sulfides	3.5	5.7	4.6	8.0	0.2	4.5	8.2	7.2
Phosphates	0.2	1.0	0.6	0.4	0.7	0.6	0.2	0.5
Phlogopite	0.2	0.5	0.4	n.d.	n.d.	n.d.	n.d.	n.d.

LAP 04840 data from classification of EMP maps of characteristic X-ray emissions. See Section 2 for details of analyses and classification. LAP 04840 data reported as area proportions and are assumed to be equivalent to volume proportions (see text). Other data reported as volume proportions.

Data from other meteorites as follows: Rumuruti (Schulze et al., 1994); Acfer 217 (Bischoff et al., 1994); ALH 85151 and Carlisle Lakes (Kallemeyn et al., 1996); PCA 91002 (Rubin and Kallemeyn, 1994).

[a] N.d., not detected.

2. SAMPLES AND METHODS

Samples of LAP 04840 were obtained by request from the Meteorite Working Group of ANSMET (Antarctic Search for Meteorites), and the Meteorite Curator at Johnson Space Center, Houston, Texas. Most of the analyses here were done on thin section LAP 04840,30 and some images are from section LAP 04840,23. Mössbauer analyses were obtained from bulk powders and mineral separates from a chip of LAP 04840, which is being used for optical spectral analyses (Klima et al., 2007).

2.1. Electron microprobe analysis

Major and minor element analyses of minerals in LAP 04840 were obtained with the Cameca SX-100 electron microprobe at the ARES Division of the Johnson Space Center (JSC). Electron accelerating potential was 15 kV, and other conditions were varied according to mineral group.

Olivines, pyroxenes, oxides, and sulfides were analyzed with a beam of 20 nA current (measured in a Faraday cup), and focused onto the sample, yielding an analytical area of ~1–2 μm diameter. Counting times were 30 s on peak. Natural minerals and synthetic oxide standards were used for calibration, including variously kaersutite, $A1_2O_3$, Fe_2O_3, TiO_2, MgO, NiO, chromite, wollastonite, tephroite, almandine, and troilite. Element maps and back-scattered electron images (BSE) were collected under these conditions. Amphiboles were analyzed as for other mafic oxides, but with tugtupite as a Cl standard and Durango apatite as an F standard. The F standardization was verified against synthetic fluor-phlogopite.

Albite and apatite were analyzed under relatively gentle conditions, 5 nA beam current, and a beam defocused to 5 μm diameter on the section surface, to reduce element volatilization and mobility. Standards for the LAP 04840 albite included Amelia albite, adularia, wollastonite, and andradite for Fe. Counting times were 30 s on peak. Standards for apatite were: Durango apatite for Ca, P, and F; tugtupite for Cl; troilite for S; and kaersutite for Fe, Mg, Si, and Na. Fluorine was analyzed using the PC1 multilayer crystal, at a count time of 60 s on peak. Other counting times were 30 s on peak.

2.2. Hydrogen isotope and volatile element abundance analyses

The D/H ratios and volatile element abundances (H, C, F, S, and Cl) in the magnesiohornblende and phlogopite were measured at the Department of Terrestrial Magnetism, Carnegie Institution of Washington using a Cameca IMS-6f ion microprobe (SIMS). Operating conditions for H isotope measurements were: 15 kV Cs^+ primary beam of 4–5 nA, −5 kV secondary accelerating voltage, a 50-eV energy window, a 75-μm imaging field, a mass resolution of ~400, an electron flood gun for charge compensation, and a 50-μm field aperture. The primary beam was rastered over an area that was larger than the image of the field aperture so that only ions generated from the central portion of the sputter crater were measured. Pre-sputtering of the samples for 5–10 min prior to analysis was used to reduce surface contamination. For each measurement cycle, count rates were measured for H and ^2H for 1 and 10 s, respectively. A total of 40 cycles were collected for each analysis. A number of terrestrial amphiboles and biotites of known composition were used to determine the instrumental mass fractionation (IMF) factors: $-189 \pm 12‰$ for magnesiohornblende and $-87 \pm 31‰$ for phlogopite (uncertainty 1 standard deviation). The quoted errors for the LAP 04840 amphiboles and phlogopites include the internal precision of the measurements and the uncertainties in the instrumental mass fractionation factors.

Similar conditions were used for the measurement of volatile element abundances, except a mass resolution of ~5000 was used. For each measurement cycle, count rates were monitored for ^{12}C, ^{16}OH, ^{19}F, ^{30}Si, ^{32}S, ^{35}Cl. Counting times for each mass during each cycle were 5 s, except for ^{12}C which was 10 s, and a total of 5 cycles were collected at each point. A series of standard silicate glasses with a range of volatile contents were measured to determine calibration curves for, for instance, H_2O (wt%) vs. $^{16}OH/^{30}Si$ ratio. Standardization data are available by request.

2.3. Mössbauer analysis

Splits of powdered meteorite for Mössbauer analysis were obtained from a 1.147-g chip of LAP 04840 provided by the Meteorite Working Group at the JSC Astromaterials Acquisition and Curation Office. Half of the chip was ground under distilled water to prepare for Mössbauer analysis while the other half was retained for further spectroscopic study. A portion of the Mössbauer split of the powdered sample was used to obtain whole rock spectra. The remaining powders were hand-picked under a binocular microscope. Separated fractions included an olivine-rich fraction (8 mg) with minor orthopyroxene, an amphibole-rich fraction (2 mg, with minor olivine and pyrrhotite), and a mica fraction (1 mg with minor olivine). Each fraction was then gently crushed under acetone before mixing with a sugar–acetone solution designed to form sugar coatings around each grain and prevent preferred orientation. Grains were gently heaped in a sample holder confined by kapton tape.

Mössbauer spectra were acquired at 295 K using a source of ~60 mCi ^{57}Co in Rh on a WEB Research Co., Model WT302 spectrometer (Mount Holyoke College). For each sample, the fraction of the baseline due to the Compton scattering of 122 keV gammas by electrons inside the detector was subtracted. Run times were 12–24 h, and baseline counts were ~2 million after the Compton correction, as needed to obtain reasonable counting statistics. Spectra were collected in 1048 channels and corrected for nonlinearity via interpolation to a linear velocity scale defined by the spectrum of the 25 μm Fe foil used for calibration. Data were then folded before fitting.

All samples were initially run at a velocity scale of ±4 mm/s. When it became clear that pyrrhotite sextets were present, the whole rock samples were also re-run at an expanded velocity setting of ±12 mm/s to check for the

presence of other iron oxides such as magnetite. No features representing either nano-phase or larger magnetite were observed, suggesting that the sample studied contained magnetite at a level of <1% of the total Fe in the sample.

To model the data with the sextets of magnetic minerals, we used the computer program MexfielDD, an unpublished code developed at the University of Ghent (Belgium). MexfielDD uses Lorentzian line shapes and has the capability to solve the full Hamiltonian. Isomer shift, quadrupole splitting, line width, and doublet area were generally allowed to vary freely in the fits, though constraints were used rarely to ensure that line width did not fall below ~0.22 mm/s. Errors on isomer shifts are estimated at ±0.04 mm/s because of peak overlap. Quadrupole splitting values are ±0.05 mm/s. The distribution of area among multiple Fe^{2+} doublets is probably ±5–10% absolute.

The mineral separate results are presented in the individual mineral sections. The Mössbauer parameters are consistent from sample to sample, but it is difficult to assign most of the spectral doublets to specific minerals because most of the target minerals (pyroxene, magnesiohornblende, and phlogopite) have very similar octahedral site geometries, and thus similar Mössbauer parameters. Furthermore, olivine and orthopyroxene are very similar in color, and thus impossible to distinguish by hand-picking. Finally, the abundance of olivine relative to the hydrous phases in the sample made it very difficult to hand-pick magnesiohornblende or phlogopite separates without a small amount of olivine contamination. Fortunately, the olivine doublets are easily distinguished in these spectra because of their higher quadrupole splittings relative to the other phases present.

2.4. Oxygen isotope analyses

Oxygen isotope analyses were performed on bulk rock samples, chips and loose grains, following the procedures of Rumble et al. (2007). Samples were crushed gently to a grain size of 0.5 mm in a boron nitride mortar and pestle under ethanol, and were then washed in DI H_2O, soaked and intermittently ultrasonicated in dilute HCl, washed in DI H_2O, and dried. Samples were weighed in ~2 mg aliquots, loaded in the fluorination chamber, and fluorinated repeatedly for 24 h at room temperature until there was no release of non-condensable gas by spontaneous fluorination reactions. Once the blank and terrestrial contamination had been removed, oxygen was liberated quantitatively by heating samples with a 25-W Synrad CO_2 laser under 30 torr of BrF_5. Oxygen was purified from contaminants such as NF_3 and CF_4 over a substrate of molecular sieve 5A and loaded into a Thermo-Electron MAT 252 mass spectrometer. Each analysis was monitored for contamination by mass scanning for H_2O, N_2, NF_3, and CF_4. The results were standardized against a Gore Mountain garnet (USNM 107144).

2.5. Modal analysis calculations

Modal mineral abundances in LAP 04840 were estimated from maps of characteristic X-ray emissions made with the SX-100 electron microprobe. Two maps were made of disjunct areas, each 700 by 700 pixels (490,000 pixels); the analyzed spots on map 1 were separated by 5 μm (total map area = 12.25 mm^2), those on map 2 were separated by 10 μm (49 mm^2), thereby covering the majority of the thin section. Count time on each spot was 10 ms. The raw map data were imported into the image processing software ImageJ, and a histogram of values produced for each element map. Unique peaks were assigned to specific minerals based on quantitative mineral analysis. Mixed pixels, those where the volume of X-ray excitation included more than one phase, fall in between peaks on the histograms, and were not included in the mode calculation. Based on these mineral assignments, maps were prepared identifying each pixel as a particular mineral, and the mineral proportions were calculated from these maps using Adobe Photoshop.

3. RESULTS

3.1. General petrology and mineralogy

LAP 04840 is composed of chondrules, chondrule fragments, and mineral grains in a finely crystalline matrix (Fig. 1A). The chondrules range up to ~3 mm diameter, and include many varieties such as barred olivine, porphyritic olivine, and porphyritic pyroxene (Fig. 2B and C). Many chondrules are surrounded by rims of finely crystalline material (~20 μm grain size), comparable to fine-grained rims on chondrules in other chondrites (e.g., MacPherson et al., 1985; Metzler et al., 1991). The interchondrule matrix material is composed of anhedral grains, ~20–40 μm across in a granular polygonal texture (Fig. 2G). The chondrule/matrix volume ratio is <1.

Mineral proportions (area, from X-ray maps) in LAP 04840 are given in Table 1 for two disjunct areas of the same thin section (Fig. 1B). The modal abundance of mineral phases in LAP 04840 varies across the sample, suggesting textural heterogeneity (Table 1). The modal mineralogy of Table 1 does not distinguish between grains in chondrules or mineral fragments and those occurring in the matrix.

Mössbauer whole rock spectra (Fig. 3 and Table 2) were collected on two size fractions and are nearly identical, though the <45-μm size fraction appears to have slightly more olivine (71%) than the 45- to 125-μm fraction (65%). As a result, the former has slightly less Fe^{3+} (9%) than the latter (11%) because the olivine has the lowest Fe^{3+} content of the phases present.

An estimate of the major element composition of LAP 04840 (Table 3) was calculated from EMP and SIMS analyses of minerals (Tables 4, 5) and the mineral proportions of Table 1. We took area proportions as equivalent to volume proportions (implicitly assuming that the rock is isotropic), and converted from volume to mass proportions by estimated densities, based on mineral compositions in Tables 4 and 5, and density ranges in Deer et al. (1983). The calculated bulk composition is similar to those of other R chondrites (Table 3), and of non-carbonaceous chondrites in general.

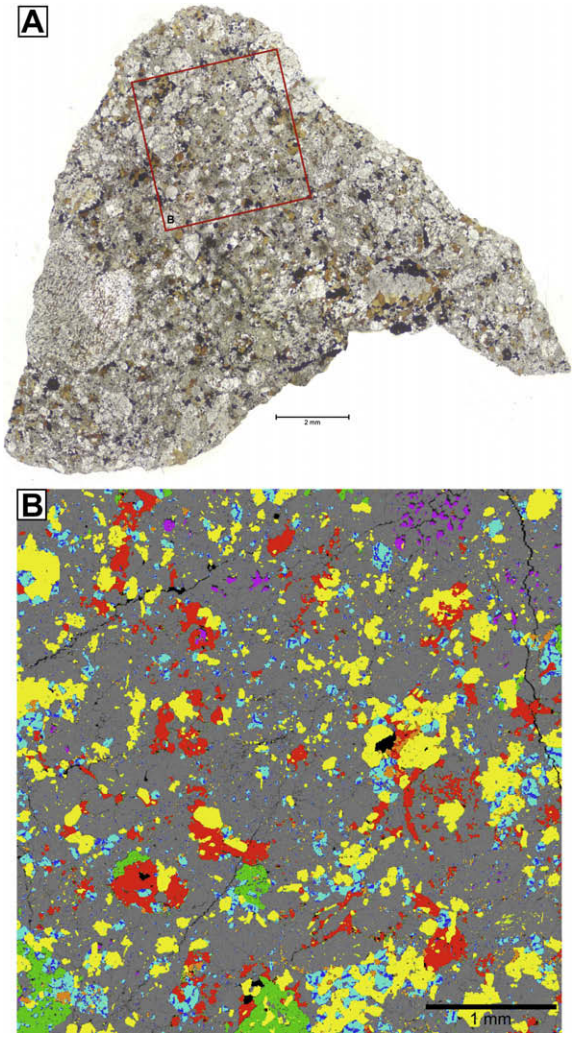

Fig. 1. LAP 04840, thin section 30. Whole thin section plane polarized light, mosaic of digital images, exposed area ~1.5 cm across. Note large radial-olivine chondrule at left edge of section, and porphyritic olivine–pyroxene chondrule just left of the top of the section. Brown grains are hornblende and phlogopite; white (clear) grains are mostly olivine and orthopyroxene; black (opaque) material is magnetite and Fe–Ni sulfides. Box denotes location of map in (B). (B) Mineral map of a portion of the thin section near the top of Fig. 1A, 700 μm square, based on EMP element maps (see text). Color mapping is: gray, olivine; yellow, amphibole; green, pyroxene; red, plagioclase; purple, biotite; dark blue, oxides; light blue, sulfides; and orange, apatite.

Many olivines throughout the sample exhibit undulatory extinction and irregular fractures indicative of shock stage S2 as defined by Stoffler et al., 1991. The albite in LAP 04840 exhibits undulatory extinction as well, indicating S2 conditions. There is no evidence in the albite of higher order shock deformation, like reduced birefringence or shock twinning.

3.1.1. Olivine

Olivine, the most abundant mineral in LAP 04840, dominates the matrix, and occurs in chondrules and isolated grains (Figs. 1 and 2B, C, and G). In chondrules, olivine grains are as large as hundreds of micrometers in length, and are anhedral through subhedral in shape (the latter are probably relict phenocrysts). Matrix olivine grains are 10–40 μm across, are equigranular without crystallographic control, and form a granular polygonal mosaic (Fig. 2G). Despite size and texture differences, the olivine is compositionally homogeneous (within analytical uncertainty) among different chondrules, between chondrules and isolated grains, and within the groundmass. The average olivine composition in LAP 04840 is $Fo_{62}Fa_{38}$, and does not vary significantly (analyses are consistent within 2σ of a constant value) across grains as large as 0.5 mm (Table 4 and Fig. 5). The olivine composition measured in this meteorite is similar to the average values of other R chondrites. However, some R chondrites show much wider ranges of olivine compositions (Bischoff et al., 1994; Rubin and Kallemeyn, 1994; Schulze et al., 1994; Kallemeyn et al., 1996), which reflects either the presence of clasts of unequilibrated material (e.g., R3–R6), or, in the case of some samples (ALH 85151 and PCA 91002), incomplete equilibration.

The Mössbauer spectrum of the olivine separate (Fig. 4 and Table 2) is dominated by two doublets, isomer shift $\delta = 1.10$ and 1.18 mm/s and quadrupole splitting $\Delta = 2.96$ and 2.85 mm/s. respectively. These represent Fe^{2+} in the M1 and M2 sites. An additional doublet, ~6% of the total Fe^{2+} has a δ of 1.13 mm/s and Δ of 2.08 mm/s and is assigned to orthopyroxene. Finally, an additional ~5% of the Fe in the separate appears in a doublet with parameters consistent with Fe^{3+}. Because orthopyroxene rarely contains >10% of its total Fe as Fe^{3+}, this doublet is assigned to the olivine. The amount of Fe^{3+} in olivine is analogous to what is observed in metasomatized, amphibole-bearing mantle xenoliths (McGuire et al., 1991); however, EMP chemical analyses normalize properly to olivine stoichiometry without requiring any Fe^{3+}.

3.1.2. Pyroxene

All pyroxene in LAP 04840 is orthopyroxene (Table 4); we have not found any Ca-rich pyroxene. Orthopyroxene occurs both in chondrules and as isolated mineral fragments, and its abundance varies significantly across the thin section (Table 1). Most orthopyroxene grains are anhedral and smaller than 100 μm, although a few chondrules contain subhedral grains (possibly relict phenocrysts) as large as several hundred μm. The orthopyroxene is compositionally homogeneous, at $Wo_1En_{69}Fs_{30}$: $Ca_{0.02}Mg_{1.36}Fe^{2+}_{0.60}Mn_{0.01}Al_{0.01}Si_2O_6$ (Table 4), with both more rapid diffusing elements (i.e., Mg and Fe) and slower diffusing elements (i.e., Al) showing no variations within uncertainty. Orthopyroxene Mg# values fall at the upper end of the range analyzed in other R chondrites (Fig. 6). However, orthopyroxenes in other R chondrites show much wider ranges of Mg# than does LAP 04840 (Fig. 6: Bischoff et al., 1994; Rubin and Kallemeyn, 1994; Schulze et al., 1994; Kallemeyn et al., 1996). The variability in orthopyroxene compositions may reflect the presence of lithic clasts of varying petrologic grades (R3–R6) present in the other R chondrites.

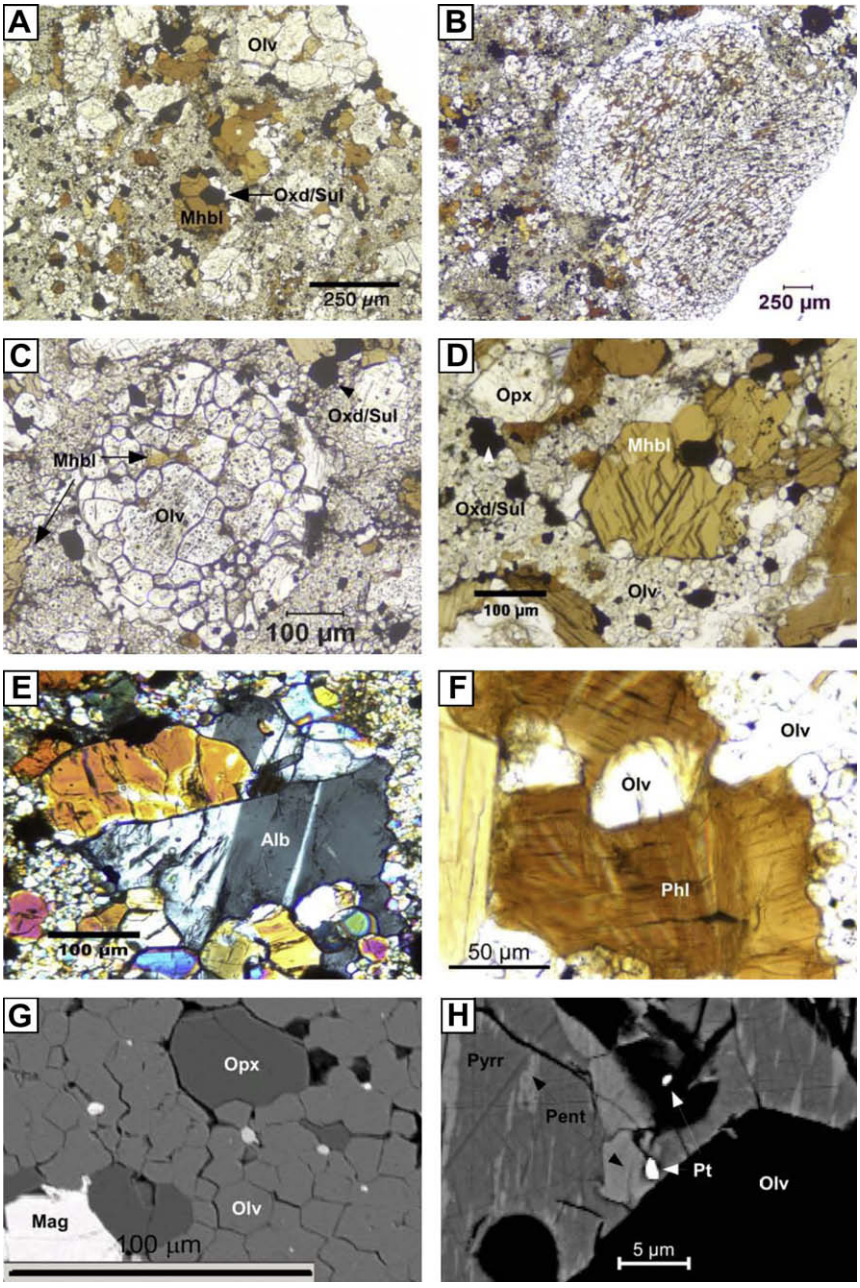

Fig. 2. (A) General texture in thin section. Amphibole (magnesiohornblende: Mhbl), olivine (Olv), and oxide–sulfide intergrowths (Oxd–sul), plane polarized light. Circular, coarser-grained chondrules are set in fine-grained matrix, mostly of olivine and with widely distributed grains of amphibole. Chondrules show a wide range of texture and compositions, from nearly pure amphibole, to nearly no amphibole. (B) Radial olivine chondrule, plane polarized light. The brown mineral scattered throughout the chondrule is magnesiohornblende. (C) Well-defined olivine chondrule, plane polarized light. Comparison between (B) and (C) illustrates the range of chondrule sizes in the section. (D) Magnesiohornblende grains, plane polarized light. Grain at center shows characteristic 56° intersections of cleavage planes. The range of color tones among magnesiohornblende grains indicates its pleochroism. Other minerals include orthopyroxene (Opx), olivine, and oxide–sulfide intergrowths. Note magnesiohornblende grains at lower left, outlining the arc of a chondrule border. Image taken from thin section LAP 04840,23. (E) Twinned albite grains (Alb), crossed polarized light. Surrounding the albite are subhedral grains of olivine and orthopyroxene. (F) Phlogopite grain (Phl), with cleavage plane oriented approximately perpendicular to section surface (thin section 23); plane polarized light. Note bent and deformed cleavage traces. (G) Groundmass texture, BSE image, mostly of olivine. Anhedral grains with straight boundaries, and grain edge angles approximating 120° suggest textural equilibrium. (H) BSE image of rare Pt metal associated with sulfides (pyrrhotite, Pyrr and pentlandite, Pent).

3.1.3. Albite

Albite occurs as subhedral mineral fragments, with widths of $\leqslant$350 μm, throughout LAP 04840—in the matrix, as isolated mineral grains, and among olivine and pyroxene in chondrules. The albite grains show normal birefringence (to first-order in the thin section), and show both simple

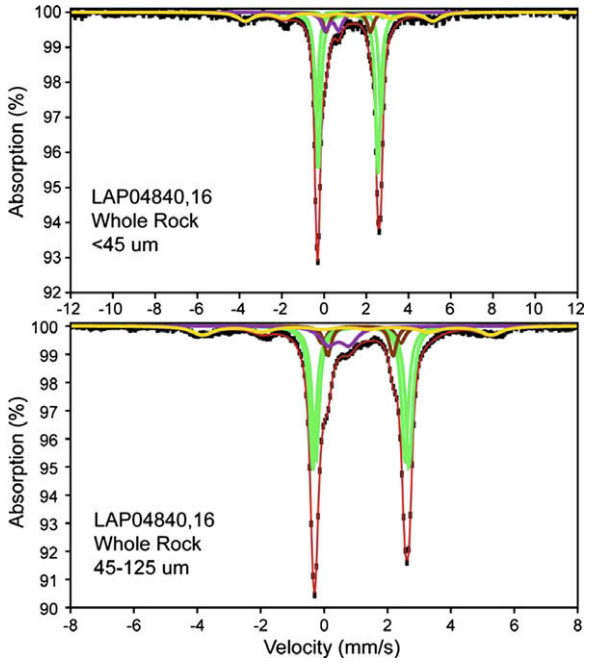

Fig. 3. Mössbauer spectra of two different size fractions of the whole rock from LAP 04840,16. Pyrrhotite is gold, olivine is green, and orthopyroxene and amphibole are brown. Although a spinel-phase oxide is present and it contains significant proportion of magnetite component (Table 4), the Mössbauer spectrum lacks the characteristic sextet of magnetite, i.e., peaks at, for example, −7.6 and 4.8 mm/s. The absence of these peaks above the Mössbauer detection limits may reflect the low abundance of magnetite (Table 1) and possibly a heterogeneous distribution in the meteorite.

and polysynthetic twinning (Fig. 2E). Albite compositions in LAP 04840 are constant within 2σ uncertainty at a value of $An_8Ab_{90}Or_2$ (Table 4).

3.1.4. Ferri-magnesiohornblende

The amphibole in LAP 04840 is pleochroic from tan to brown in color, and shows two strong cleavages at 56° to each other (Fig. 2D). Its grains are euhedral to subhedral, up to several hundred μm across in thin section, and are widely distributed throughout the meteorite (Fig. 1) in chondrules, chondrule fragments, and the matrix. Magnesiohornblende in chondrules is concentrated among the subhedral olivine and orthopyroxene crystals, in what would have been mesostasis or glass in 'normal' chondrules.

The average composition of the amphibole from EMP and SIMS analyses is classified as ferri-magnesiohornblende (Fig. 7 and Table 5), according to the IMA scheme (Leake, 1997; Hawthorne and Oberti, 2007); it contains relatively abundant hydroxyl, and very little F or Cl (Table 6). The average analysis is cast as a structural formula by first normalizing element abundances to 13 small cations (not including Ca, Na, and K; Cosca et al., 1991). This calculation assumes that the tetrahedral (T) and octahedral (M1–M4) sites are fully occupied, and that the M4 site contains only Ca and Na; these assumptions seem reasonable for a calcic–sodic amphibole like that in LAP 04840. Aluminum is assigned first to fill the tetrahedral sites. Some analyses show Al beyond that for full occupancy of the tetrahedral sites, and that Al is assigned to octahedral sites. Conversely, some analyses require a small proportion of $^{IV}Fe^{3+}$ for full

Table 2
Mössbauer parameters for LAP 04840

Sample	Mineral	I.S.	Q.S.	Area
Olv + Opx	Olv Fe^{2+}	1.18	2.96	53
	Olv Fe^{2+}	1.10	2.85	36
	Opx Fe^{2+}	1.13	2.08	6
	Olv ? Fe^{3+}	0.28	0.40	5
	Olv Fe^{2+}	1.15	2.92	48
Amph[a] + Olv	Amph Fe^{2+}	1.04	2.59	5
	Amph Fe^{3+}	0.36	0.97	17
	Amph Fe^{3+}	0.20	0.35	11
	Olv Fe^{2+}	1.19	2.89	31
Phlog + Olv	Phlog Fe^{2+}	1.13	2.65	23
	Phlog Fe^{3+}	0.30	1.23	15
	Phlog Fe^{3+}	0.30	0.46	31
	Olv Fe^{2+}	1.17	3.04	34
Whole rock[a] 45–125 μm	Olv Fe^{2+}	1.15	2.81	32
	Opx or Amph Fe^{2+}	1.18	2.49	5
	Opx or Amph $^{2+}$	1.14	2.06	7
	Fe^{3+}	0.46	0.65	9
	Olv Fe^{2+}	1.17	3.06	25
Whole rock[a] < 45 μm	Olv Fe^{2+}	1.36	2.87	1
	Olv Fe^{2+}	1.14	2.83	45
	Opx or Amph Fe^{2+}	1.15	2.10	7
	Fe^{3+}	0.38	0.38	7

Olv, olivine; opx, orthopyroxene; amph, amphibole; and phlog, phlogopite.
[a] Sample also contains pyrrhotite, with MS parameters of I.S. = 0.70 mm/s, Q.S. = 2.80 mm/s and BHf = 28.2 T.

Table 3
Bulk compositions of selected R chondrites

	LAP 04840	Rumuruti	Acfer 217	Carlisle lake	ALH 85151	PCA 91002
SiO_2	36.87	*39.12*[a]	*39.94*	*36.98*	*38.78*	*37.48*
TiO_2	0.12	NM[b]	0.15	NM	NM	NM
Al_2O_3	2.04	1.93	1.93	2.08	2.08	2.10
Cr_2O_3	0.80	0.54	0.56	0.53	0.52	0.50
Fe_2O_3	2.86	NM	NM	NM	NM	NM
FeO	27.45	31.47	32.04	31.01	30.49	31.01
NiO	1.77	1.44	0.41	1.38	1.44	1.38
MnO	0.33	0.29	0.28	0.30	0.29	0.30
MgO	23.09	20.66	20.10	22.06	21.56	22.55
CaO	1.66	1.54	1.54	2.71	1.90	1.75
Na_2O	0.84	0.92	0.93	0.86	0.87	0.86
K_2O	0.08	0.09	0.12	0.09	0.07	0.07
P_2O_5	0.22	NM	NM	NM	NM	NM
F	0.00	NM	NM	NM	NM	NM
Cl	0.01	NM	NM	NM	NM	NM
S	2.05	*2.00*	*2.00*	*2.00*	*2.00*	*2.00*
	100.20	*100.00*	*100.00*	*100.00*	*100.00*	*100.00*

Data reported as weight percent oxide. LAP 04840 data were estimated from mass balance calculations. Other meteorite data taken from Schulze et al. (1994) [Rumuruti], Bischoff et al. (1994) [Acfer 217], Rubin and Kallemeyn (1989) [Carlisle Lake, ALH 85151], and Rubin and Kallemeyn (1994) [PCA 91102].
[a] Values in italics are estimated or by difference.
[b] NM, not measured.

Table 4
Mineral compositions (except amphibole) in LAP 04840

	Olivine	Pyroxene	Albite	Phlogopite	Magnetite	Apatite
SiO_2	36.02 (0.14)	53.96 (0.29)	66.23 (0.63)	39.23 (0.39)	0.05 (0.04)	0.07 (0.12)
TiO_2	0.02 (0.02)	0.02 (0.02)	NM	0.95 (0.10)	1.26 (0.06)	NM
Al_2O_3	0.02 (0.02)	0.14 (0.02)	22.12 (0.35)	13.83 (0.19)	2.28 (0.05)	NM
Cr_2O_3	0.02 (0.02)	0.05 (0.02)	NM	0.85 (0.01)	19.07 (0.33)	NM
FeO[a]	32.98 (0.30)	19.4 (0.20)	0.32 (0.11)	11.96 (0.07)	70.19 (0.73)	0.49 (0.13)
NiO	0.36 (0.03)	0.13 (0.02)	NM	0.42 (0.05)	0.33 (0.08)	NM
MnO	0.43 (0.03)	0.42 (0.02)	NM	0.06 (0.02)	0.25 (0.03)	NM
MgO	29.56 (0.17)	24.72 (0.08)	NM	18.53 (0.48)	1.62 (0.06)	0.11 (0.03)
CaO	0.04 (0.02)	0.48 (0.04)	1.55 (0.16)	0.03 (0.01)	0.27 (0.39)	52.55 (0.54)
Na_2O	0.01 (0.01)	0.02 (0.01)	9.89 (0.25)	1.45 (0.09)	NM	0.11 (0.04)
K_2O	NM[b]	NM	0.41 (0.05)	7.53 (0.18)	NM	NM
P_2O_5	NM	NM	NM	NM	NM	42.20 (0.54)
F	NM	NM	NM	0.04	NM	0.03 (0.03)
Cl	NM	NM	NM	0.08	NM	1.99 (0.07)
H_2O	NM	NM	NM	4.25	NM	NM
SO_3	NM	NM	NM	NM	NM	0.04 (0.06)
O = F,Cl	NM	NM	NM	NM	NM	−0.46 (0.02)
Sum	99.45	99.33	100.52	94.84	95.31	97.13
	Fo 61.6	Wo 1.0	Ab 89.8		Mg 60.6	
	Fa 38.4	En 68.7	An 7.8		Sp 8.7	
		Fs 30.3	Or 2.4		Chr 27.3	
					Usp 3.4	
N[c]	183	24	89	10	28	20

Major element totals are recorded as oxide weight percent. Numbers in parentheses indicate the standard deviation among sample analyses. Volatile species measured using SIMS are recorded as weight percent element (F and Cl) or oxide (H_2O). Normalizations as follows: olivine and magnetite to three cations, pyroxene to four cations, albite to five cations, apatite to 13 anions.

[a] All Fe as FeO.

[b] Element not measured.

[c] Number of analyses.

T-site occupancy. The A site is partially occupied with Na and K. The SIMS analyses of H, F, and Cl, imply slightly insufficient OH, F, and Cl to fill the halogen site, so the remainder is assigned to O^{2-} (although the proportion of O^{2-} may be within analytical uncertainty of the H analyses). Finally, ferric iron is calculated by charge balance, yielding $Fe^{3+}/Fe_{tot} = 78\%$ and the following structural formula: $(Na_{0.38}K_{0.05})(Ca_{1.53}Na_{0.47})(Cr_{0.09}Ti_{0.05}Mg_{3.55}Fe^{2+}_{0.29}Fe^{2+}_{0.99}Mn_{0.02}Ni_{0.02})(Si_{6.85}Al_{1.10}Fe^{3+}_{0.05})O_{22}(OH_{1.92}F_{0.01}Cl_{0.01}O_{0.06})$ (Table 5 and Fig. 7A).

The Mössbauer spectrum of the magnesiohornblende confirms the ferric iron abundance estimated from EMP analyses. The Mössbauer spectrum of the magnesiohornblende separate shows peaks ascribed to small proportions of olivine and pyrrhotite (Fig. 4 and Table 2). Mössbauer doublets from olivine represent 48% of the Fe in the mineral separate even though the separate is mostly hornblende, because a volume of olivine contains three times the Fe in a volume of hornblende. Because the olivine has $Fe^{3+}/Fe_{tot} = \sim 5\%$ (see above), Fe^{3+} in the olivine must amount to ~2–3% of the total Fe in the hornblende spectrum. The remaining Fe^{3+} is ascribed to the magnesiohornblende, which implies that it has $Fe^{3+}/Fe_{tot} = \sim 80\%$. This value is entirely consistent with average $Fe^{3+}/Fe_{tot} = \sim 78\%$ inferred from EMP and SIMS analyses and crystal chemistry (Table 5).

The average composition of the amphibole in LAP 04840 is near the ferric equivalent of magnesiohornblende, ferri-magnesiohornblende, $\square(Ca_2)(Mg_4Fe^{3+})(Si_7Al)(OH)_2$ (Fig. 7A and B), as defined by the IMA classification scheme (Leake, 1997; Hawthorne and Oberti, 2007). The average chemical analysis (Table 5) is rich in Na, and falls close to the boundary between the calcic amphibole ferri-magnesiohornblende and the sodic–calcic amphiboles (Fig. 7B). Several analyses plot in the edenite and ferri-barroisite fields (Fig. 7A and B). The variability in amphibole chemical compositions can be described by small proportions of the coupled substitutions Fe^{2+}–Mg (on the octahedral site), Fe^{3+}–Al (on the tetrahedral site) (ferri-tschermakite coupled substitution $[^{VI}Fe^{3+} + {}^{IV}Al \leftrightarrow {}^{IV}Si + {}^{VI}Mg]$), and K–Na (on the A crystallographic site). However, the majority of the variability is related to variations in the Na distribution between the M4 and A crystallographic sites (Fig. 7B). This suggests edenite ($^{A}Na + {}^{IV}Al \leftrightarrow {}^{A}\square + {}^{IV}Si$) and richterite ($^{A}Na + {}^{M4}Na - \leftrightarrow {}^{A}\square + {}^{M4}Ca$) coupled substitutions are predominant.

SIMS analyses of magnesiohornblende grains were made on nine total spots in seven different crystals and give an average $\delta D = +3660 \pm 75‰$.

3.1.5. Phlogopite

On average, 0.4% of LAP 04840 is phlogopite (Table 1), mostly in small (<100 μm) anhedral to subhedral grains, which are pleochroic in browns. Phlogopite is distinguished from magnesiohornblende in thin section by its single cleavage direction, deformed cleavage and associated dispersion of extinction direction, and less pronounced pleochroism (Fig. 2F).

Table 5
Amphibole compositions in LAP 04840

	Average	Edenite	Barroisite
SiO_2	47.71 (0.87)	46.59 (0.57)	49.23
TiO_2	0.47 (0.09)	0.53 (0.04)	0.55
Al_2O_3	6.41 (0.48)	6.91 (0.08)	6.97
Cr_2O_3	0.74(0.11)	0.82 (0.05)	0.79
Fe_2O_3	7.83 (0.29)	8.52 (0.17)	9.72
FeO	4.00	3.11	3.84
MnO	0.13 (0.02)	0.13 (0.03)	0.12
MgO	16.58 (0.40)	16.33 (0.28)	15.79
CaO	9.96 (0.11)	9.98 (0.07)	9.78
Na_2O	3.01 (0.13)	3.28 (0.07)	2.36
K_2O	0.25 (0.02)	0.27 (0.01)	0.32
F[a]	0.03	0.03	0.03
Cl[a]	0.04	0.04	0.04
F, Cl=O	−0.02	−0.02	−0.02
H_2O[a]	2.00	2.00	2.00
Sum	99.14	98.50	101.50
Structural formulae, normalized to 13 small cations			
T sites			
Si	6.872	6.751	6.993
Al^{IV}	1.088	1.180	1.007
Fe^{3+}	0.040	0.069	0.000
M1–M3 sites			
Al^{VI}	0.000	0.000	0.160
Cr	0.084	0.094	0.088
Ti	0.050	0.058	0.059
Mg	3.559	3.527	3.344
Fe^{2+}	0.482	0.377	0.456
Fe^{3+}	0.809	0.860	0.879
Mn	0.016	0.016	0.014
M4 site			
Ca	1.538	1.549	1.488
Na	0.462	0.451	0.512
A site			
Na	0.377	0.471	0.137
K	0.046	0.049	0.057
Halogen site			
F	0.014	0.014	0.013
Cl	0.010	0.010	0.010
OH	1.923	1.935	1.897
O	0.053	0.041	0.080
Fe^{3+}/Fe_{tot}	0.64	0.71	0.66
N[b]	100	7	1

Values in parentheses are 1σ standard deviation. The barroisite is a single analysis.
O in halogen site calculated to fill the site; Fe^{3+} and Fe_2O_3 then calculated by charge balance.
[a] Averages from all SIMS analyses.
[b] Number of analyses.

Phlogopite grains are of nearly identical major element composition across the thin section (Table 4). To present the average chemical analysis as a structural formula, we first normalized it to fourteen small cations (Essene, 1989), assuming full occupancy of all T and M cation sites. The Fe^{3+}/Fe_{total} ratio cannot be constrained from EMP/SIMS data and stoichiometry alone, and therefore is constrained from Mössbauer measurements.

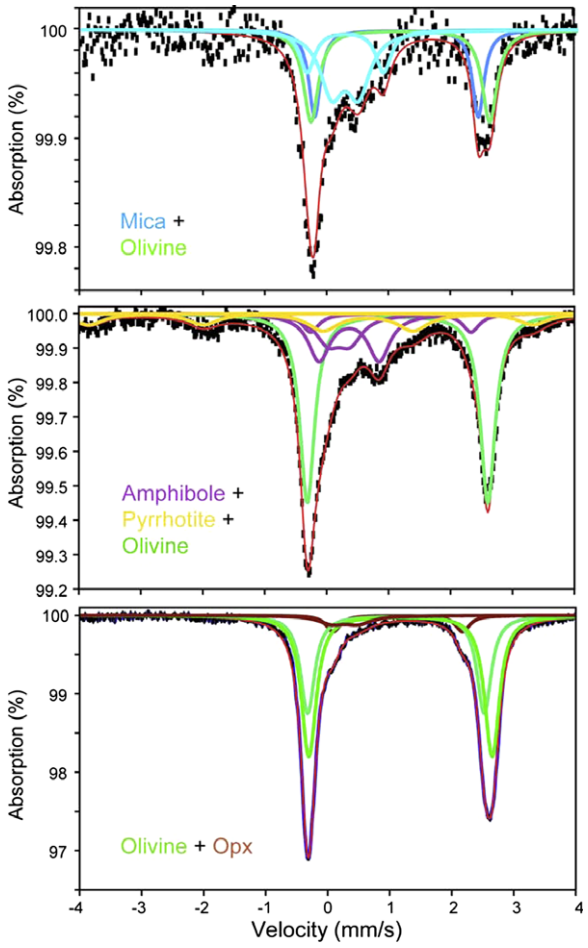

Fig. 4. Mössbauer spectra of separates of (A) biotite, (B) amphibole + pyrrhotite, and (C) olivine + orthopyroxene. Doublets are labeled by color as indicated.

The phlogopite has a high Fe^{3+}/Fe_{total} as constrained by Mössbauer data. The Mössbauer spectrum of the phlogopite mineral separate has doublets that are assigned to phlogopite and to olivine (Fig. 4 and Table 2). The olivine Fe^{2+}doublets represent 31% of the total Fe in the phlogopite sample. The olivine has $Fe^{3+}/Fe_{total} = \sim 5\%$, so that ~1–2% of the area of the Fe^{3+} doublet can be assigned to olivine. The remaining area of the Fe^{3+} doublet and the area of the Fe^{2+} doublet assigned to phlogopite, imply that the phlogopite has $Fe^{3+}/Fe_{total} = \sim 65\%$. This cation normalization yields a total cation charge in excess of that expected from the structural O^{2-} and OH + F + Cl anions, so the phlogopite must contain some O^{2-} in the halogen site. The inferred formula is $(K_{1.43}Na_{0.34})(Mg_{4.12}Fe^{2+}_{0.52}Fe^{3+}_{0.97}Al_{0.27}Cr_{0.10}Ti_{0.11})(Al_{2.15}Si_{5.85})O_{20}(OH_{2.49}Cl_{0.02}F_{0.02}O_{1.47})$ (Table 4). This phlogopite is quite rich in Na compared with common terrestrial phlogopite (Fleet and Howie, 2004). The alkali site is not filled, which may suggest that Na was lost during chemical analyses, even though care was taken to minimize this problem.

SIMS analysis of the phlogopite (made on four different grains) gives an average δD of +2930 ± 100‰ (Table 6), which is significantly lower than the δD of amphibole at +3660 ± 75‰. This difference in δD is far too large to represent equilibrium

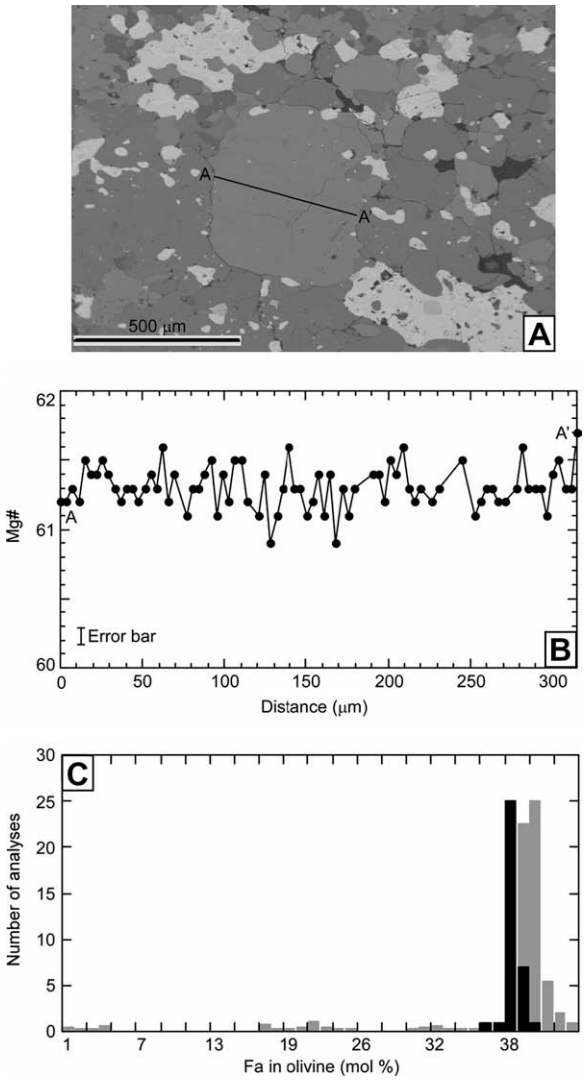

Fig. 5. (A) Discrete olivine grain in matrix (center); BSE image. Location of electron microprobe traverse from A to A′ shown. Note abundant, irregular clots rich in magnetite and sulfides (see example in Fig. 1E). (B) Plot of electron microprobe traverse A–A′ Mg#, Mg/(Mg + Fe) in percent. Error bar shown in upper left corner is 1σ for an individual analysis, and all analyses are consistent within 2σ of a constant value. (C) LAP 04840 olivine compositions, given as fayalite (Fa) %, black bars, compared to compositions in other R chondrites, gray bars (Nakamura et al., 1993; Bischoff et al., 1994; Rubin and Kallemeyn, 1994; Schulze et al., 1994; Kallemeyn et al., 1996). Fa, fayalite.

fractionation, or even kinetic fractionation *in situ*, but the SIMS analyses of the phlogopite show abundant carbon (up to 1.5%) and sulfur (to 722 ppm). Phlogopite contains little carbon or sulfur (Fleet and Howie, 2004; Tischendorf et al., 2007), so it seems likely that the analyzed high C and S abundances represent contamination. If so, the low δD of the phlogopite could also be affected by contamination, perhaps by the thin section epoxy which has $\delta D \sim -400‰$.

3.1.6. Magnetite

LAP 04840 contains a single opaque oxide mineral, magnetite, which occurs as widely dispersed grains of less than 100 μm across, and as clots of smaller grains associated with Fe–Ni sulfides, apatite, and phlogopite. The singular presence of magnetite is confirmed in other sections of LAP 04840 as well (Mikouchi et al., 2007). A single submicron chromite grain was identified in our section, but could not be analyzed due to its small size. The magnetite is chemically homogeneous across and among grains, with the average composition given in Table 4. Ferric iron in the magnetite was calculated by charge balance (i.e., three cations per four oxygens), assuming that the structure has no cation vacancies, and that iron is the only cation with multiple valence states. This procedure yields the analysis of Table 4, with a mass total that is within acceptable uncertainty of 100%. The structural formula of the magnetite is $(Fe^{2+}_{0.92}Mg_{0.09}Ni_{0.01}Mn_{0.01}Ca_{0.01})(Fe^{3+}_{1.26}Cr_{0.56}Al_{0.10}Ti_{0.04})O_4$, which can be cast in terms of end-members as $Mt_{61}Chr_{27}Sp_9Usp_3$.

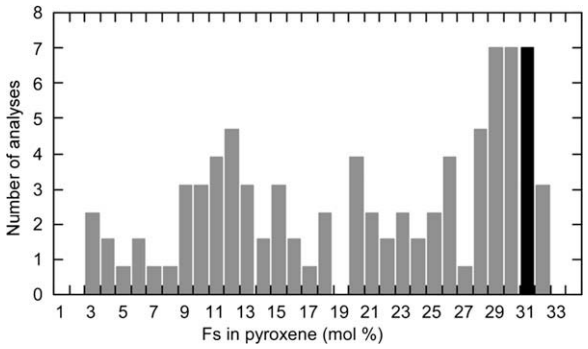

Fig. 6. Histogram of modal percent ferrosilite (Fs) component in R chondrite orthopyroxenes: LAP 04840 in black bars; other R chondrites in gray bars (Nakamura et al., 1993; Bischoff et al., 1994; Rubin and Kallemeyn, 1994; Schulze et al., 1994; Kallemeyn et al., 1996).

Mössbauer spectra of the meteorite and mineral separates show no sign of a sextet of peaks assignable to magnetite, for example, peaks at −7.6 and 4.8 mm/s (Figs. 3 and 4).

3.1.7. Sulfides

LAP 04840 contains two sulfide minerals, pyrrhotite and pentlandite, which form small grains and intergrowths (<100 μm across), and which are commonly associated with magnetite and apatite in discrete clots (Fig. 2H). Significant portions of the pyrrhotite contain fine-scale pentlandite exsolution lamellae (Fig. 2H). The sulfide grains are anhedral to subhedral, noticeably bronze-brown in reflected light, and are even brighter than the chromian magnetite in BSE contrast. The chemical analyses of the pyrrhotite and pentlandite have chemical formulae of $(Fe_{0.79}Ni_{0.12})S$ [or $(Fe,Ni)_{0.91}S$] and $(Fe_{4.23}Ni_{4.77})S_8$, respectively. The relatively high Ni content of the pyrrhotite likely reflects the fine exsolution lamellae of pentlandite, which are difficult to avoid during EMP analysis.

3.1.8. Apatite

LAP 04840 contains a small proportion (~0.6%) of apatite (Tables 1 and 4) as scattered euhedral and anhedral crystals. No merrillite was found. The chemical composi-

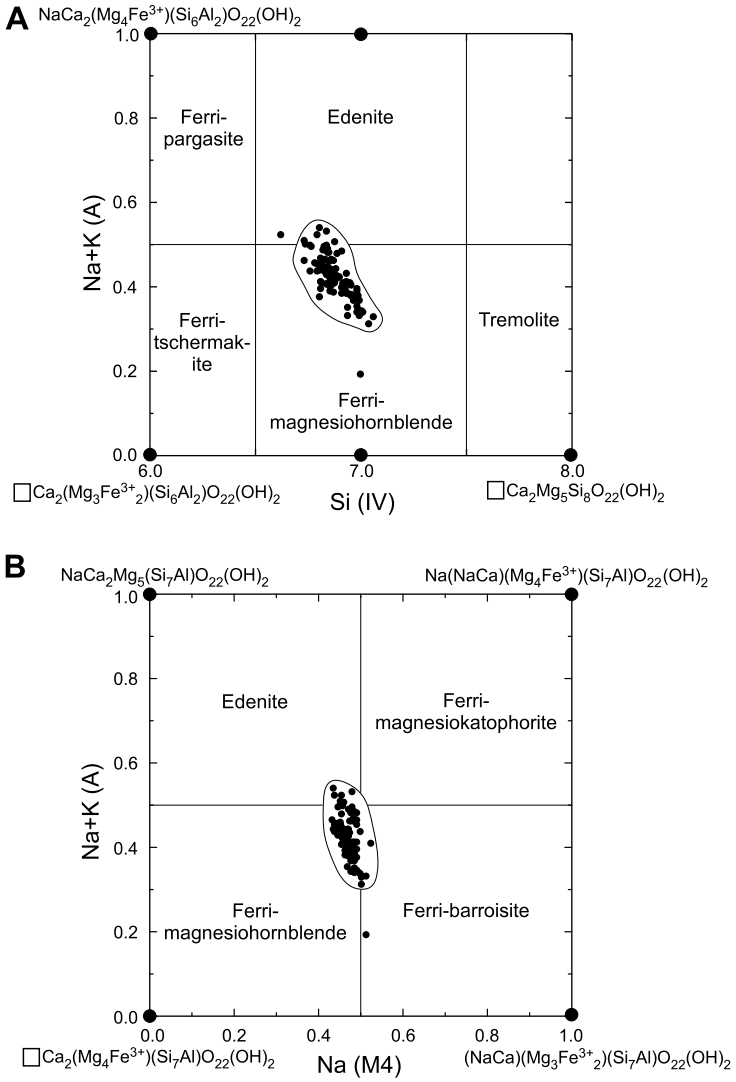

Fig. 7. Amphibole compositions of LAP 04840 per 13 small cations. (A) Amphibole crystallographic site occupancy (Si in the T-site and (Na + K) in the A-site) and the naming conventions of Leake (1997) and Hawthorne and Oberti (2007). End member compositions are on plot apices. Note the variation in A-site occupancy is primarily a function of the variation in Na site occupancy illustrated in (B). (B) Comparison of the distribution of Na between the A and M4 crystallographic sites. Although the majority of amphiboles plot as magnesiohornblendes, their compositions drape into the edenite and barroisite fields.

tion of the apatite is constant across individual grains and across the analyzed area. The structural formula of the average chemical composition was calculated assuming 13 anion charges in $Ca_5(PO_4)_3(OH,F,Cl)$ and OH was calculated by difference as $OH + F + Cl = 1$. The derived formula is $(Ca_{4.69}Na_{0.02}Mg_{0.01}Fe_{0.03})((P_{3.08}Si_{0.01}S_{0.00})O_4)_3(OH_{0.70}Cl_{0.29}F_{0.01})$, which is slightly non-stoichiometric. The high proportion of OH relative to Cl and F in the apatite is consistent with the similar proportions in the magnesiohornblende and phlogopite.

3.1.9. Rare trace phases

Several rare phases are found as submicron sized grains in LAP 04840. These include five grains of Cu metal, some with associated Zn, one grain each of lead sulfide, Ni–Fe metal, Au–Ag metal, arsenic sulfide, Pt-rich arsenic sulfide, a bismuth chloride, and an Os–Ir–Ru–Pt nugget. In addition, nine grains of Pt metal were found, all in intimate association with sulfide blebs (Fig. 2H). Grains of similar phases have been identified in other R chondrites including Rumuruti (Ni–Fe, Au, Pt, and As; Schulze et al., 1994), PCA 91002 (Cu metal; Rubin and Kallemeyn, 1994), Acfer 217 (Au, Ag, Os, and Ru; Bischoff et al., 1994), and ALH 85151 (Ni–Fe; Kallemeyn et al., 1996).

4. COMPARISON WITH OTHER R CHONDRITES

LAP 04840 has been classified as an R chondrite (Satterwhite and Righter (2006)). There are several features that warrant this classification (see Kallemeyn et al. (1996) for a thorough description of R chondrite traits). First, the oxygen isotope data indicates an affinity with previously

Table 6
SIMS analysis of LAP 04840 volatile phases

Sample	Phase	H_2O	F	S	Cl	δD
CA-1	Amphibole	1.7[a]	244.9	10.2	409.2	3716 ± 46
CA-1b	Amphibole	1.9	259.3	9.0	399.2	3716 ± 46
CA-3b	Amphibole	1.2	183.2	8.2	402.3	3743 ± 40
G-3	Amphibole	2.0	252.1	10.4	274.6	3611 ± 39
G-5	Amphibole	1.9	251.6	12.3	293.7	3638 ± 35
R-4	Amphibole	2.1	192.6	6.3	349.5	3728 ± 37
R-4b	Amphibole	2.1	260.6	4.6	315.1	3728 ± 37
R-5	Amphibole	2.2	267.8	7.3	364.8	3595 ± 39
R-6	Amphibole	2.0	261.5	5.3	315.1	3690 ± 39
Q-1	Phlogopite	5.2	424.9	192.9	833.6	2931 ± 68
Q-2	Phlogopite	4.4	376.3	213.7	677.6	2739 ± 66
Q-3	Phlogopite	6.3	443.3	722.8	874.9	3043 ± 69
R-3	Phlogopite	6.9	357.8	275.3	817.6	2776 ± 67

Sample numbers refer to location of grain within thin section.
H_2O is recorded as weight percent. Other volatiles recorded as parts per million.
[a] 1σ errors on volatile measurements were based on uncertainties in the standardization and are as follows: H_2O (16%), F (10%), S (5%), Cl (12%).

described R chondrites. The oxygen isotope results are given in Table 7 and shown in Fig. 8. The results of run 14-10 were reported in Satterwhite and Righter (2006); another run reported there is aberrant and not considered here. From Fig. 8, it is clear that the oxygen isotope ratios of LAP 04840 are close to those of R chondrites, but quite distinct from those of ordinary chondrites (H, L, and LL), Mars (source of the only other known meteorite with hydroxyl-bearing amphibole and biotite; Watson et al., 1994), as well as those of the Earth, Moon, and enstatite chondrites (all of which lie on the terrestrial fractionation line, TFL). All known carbonaceous chondrites with $\delta^{18}O$ comparable to LAP 04840 fall far below the TFL in $\delta^{17}O$ (Brearley and Jones, 1998). So, following Satterwhite and Righter (2006), the LAP 04840 meteorite is inferred to be an R chondrite. Oxygen in the LAP samples does have slightly higher $\delta^{17}O$ than other R chondrites with similar $\delta^{18}O$ (i.e., higher $\Delta^{17}O$), although the difference is smaller than the ranges in O isotope compositions in other chondrite groups (e.g., H chondrites, Fig. 8). If significant, the higher $\delta^{17}O$ of LAP 04840 might reflect the oxygen isotope heterogeneity of the constituents of R chondrites, and/or its more extensive interaction with H_2O than other R chondrites (Greenwood et al., 2000).

Table 7
Oxygen isotope analyses of LAP 04840 bulks

Sample	Run	$\Delta^{17}O$	$\delta^{17}O$	$\delta^{18}O$
LAP 04840,6	14-10[a]	3.250	5.755	4.763
LAP 04840,8	15-186	3.360	5.968	4.957
LAP 04840,8	15-187	3.397	5.862	4.686
Average		3.336	5.862	4.802
Std. Dev.		0.077	0.106	0.140

[a] Analyte gas showed some CF_4 contamination.

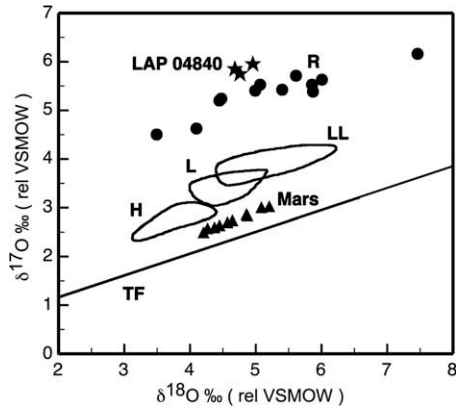

Fig. 8. Oxygen isotope composition of LAP 04840 (Table 7), compared to those of selected solar system materials. LAP 04840 shown as stars; R chondrites shown as circles; martian meteorites shown as triangles; terrestrial fractionation (TF) line includes Earth and Moon materials. Analyses of LAP 04840 plot close to those of other R chondrites, and distant from the fields of other non-carbonaceous chondrite types: H, L, LL, and E (which fall along the TFL). Data for Martian meteorites from Franchi et al. (1999); data for R chondrites from Bischoff et al. (1994, 1998b); Schulze et al. (1994); Jäckel et al. (1996); Kallemeyn et al. (1996) and Weber et al. (1997).

Second, the Mg-numbers of the silicate minerals are consistent with those measured in other R chondrites (Figs. 5 and 6). Third, the oxidation state of LAP 04840 is high as evidenced by the absence of Fe–Ni metal, the significant abundance of ferric iron in its silicate and oxide minerals, and the high NiO content of the olivine. The high oxidation state of the R chondrite class is distinct from that of the ordinary chondrites. Finally, LAP 04840 has a low chondrule to matrix volume ratio (<1) that is similar to that defined for other R chondrites. Although these data suggest that LAP 04840 belongs to the R chondrite class, the presence of the hydrous phase assemblage found in LAP 04840 makes it a unique meteorite within the R chondrites. Therefore the question arises as to the relationship between LAP 04840 and the other R chondrites. With only one hydrous sample discovered so far it is difficult to speculate on the correlation. If and when this sampling bias is resolved a more thorough examination of the extent of geologic processes active on the R chondrite parent body can be investigated and a better understanding of the relationship among the R chondrite class may be discerned.

5. METAMORPHISM

Nearly all chondrite meteorites have experienced some degree of metamorphism—chemical and textural adjustments produced by heat and/or pressure (e.g., McSween et al., 2002). Temperatures of chondrite metamorphism have been retrieved through geothermometers, although with some inconsistencies (e.g., McSween and Patchen, 1989; Wlotzka, 2005; Kessel et al., 2007). Pressures of chondrite equilibration and fugacities of volatile components, except O_2, are generally not known, as typical chondrites do not contain mineral assemblages that constrain them.

However, LAP 04840 is unique among chondrites in containing an equilibrium mineral assemblage that permits calculation of temperature, fugacity (and thus partial pressure) of a major volatile species, H_2O, and the fugacities of other volatiles like O_2, S_2, HF, and HCl. The minerals of LAP 04840 are likely to reflect chemical equilibrium at a peak pressure and temperature because they are all in mutual contact and are not chemically zoned; the exception here is that pyrrhotite and pentlandite occur as intergrowths, which may well represent re-equilibration at lower temperature. To recover temperatures and volatile fugacities at the peak of metamorphism, our major tool is the chemical equilibrium computer code THERMOCALC 3.26 (Powell and Holland, 2001), which calculates the *P–T–X* locations of mineral chemical equilibria from input mineral compositions and a self-consistent thermodynamic database and solid solution models (Powell and Holland, 1988; Holland and Powell, 1990, 1998, 2003). Activities of chemical components in minerals are calculated, except as noted, with the THERMOCALC accessory program 'AX' version 0.3 (November, 2007). Some useful equilibria involve end-member components outside of the Powell and Holland database, and some others have been located by other workers; those are taken from their defining sources.

5.1. Geothermometry

Temperature is the most crucial parameter controlling mineral assemblages in metamorphic rocks, and many mineral exchange reactions have been used as geothermometers. Only a few are useful for LAP 04840—for instance, the Ca exchange between ortho- and clinopyroxene (e.g., Lindsley and Anderson, 1983) has been applied to metamorphosed chondrites (McSween and Patchen, 1989; Slater-Reynolds and McSween, 2005), but cannot be used here in the absence of clinopyroxene. The utility of several common geothermometers applied to the LAP 04840 phase assemblage are explored below.

5.1.1. Amphibole–plagioclase

Most obviously relevant to the magnesiohornblende-bearing assemblage in LAP 04840 is the hornblende-plagioclase thermometer, based on exchange of Ca + Al for Na + Si. This exchange reaction has been explored by Holland and Blundy (1994), who cast it in terms of the end-members edenite and richterite:

$$\begin{aligned}&\text{edenite} + \text{albite} = \text{richterite} + \text{anorthite}\\&NaCa_2Mg_5Si_7AlO_{22}(OH)_2 + NaAlSi_3O_8\\&\quad = Na(CaNa)Mg_5Si_8O_{22}(OH)_2 + CaAl_2Si_2O_8 \qquad (1)\end{aligned}$$

Working from a large database of experimental and natural amphibole–plagioclase pairs, Holland and Blundy regressed the compositions with a specific algorithm to calculate Fe^{3+} in amphibole to extract solution model parameters for both minerals. With the parameters in hand, they formulated an algorithm to retrieve temperature (500–900 °C) from compositions of coexisting hornblende and plagioclase with 2σ uncertainty on the order of 50 °C.

The compositions of magnesiohornblende and plagioclase in LAP 04840 (Tables 4 and 5) yield $T = 670 \pm 60$ °C (2σ). Unfortunately, this thermometer must be seen as empirical because of its algorithm for calculating Fe^{3+} in amphibole from EMP analyses. The method we employ (above) for calculating Fe^{3+} in amphibole yields $Fe^{3+}/Fe_{tot} = 78\%$ for the LAP 04840 amphibole, in agreement with the direct measurement from Mössbauer spectra (Table 2). However, the Holland and Blundy (1994) method gives only $Fe^{3+}/Fe_{tot} = 41\%$. Although that method may yield correct temperatures, its input compositions may have incorrect Fe^{3+}/Fe_{tot} so its solid solution parameters may be incorrect.

5.1.2. Fe–Mg—olivine–orthopyroxene

The Mg–Fe exchange between olivine and orthopyroxene is sensitive to temperature. Direct experimental data are available only between 900 and 1250 °C (von Seckendorf and O'Neill, 1993), but the location of the reaction can be extrapolated to lower temperature from thermodynamic data. For the LAP 04840 olivine and orthopyroxene (Table 4), the Mg–Fe partitioning between olivine and pyroxene in LAP 04840 is greater than found by von Seckendorf and O'Neill (1993), and so implies $T < 900$ °C. The THERMOCALC program gives an equilibration temperature for the LAP 04840 olivine and orthopyroxene of ~720 °C, with a nominal 1σ uncertainty of ±260 °C. This temperature is consistent with the hornblende–plagioclase equilibrium temperature, but is so uncertain as to be of limited utility.

5.1.3. Fe–Mg—spinel–olivine–orthopyroxene

The partitioning of Fe and Mg between spinel and olivine or orthopyroxene are functions of temperature (e.g., Sack and Ghiorso, 1991; Liermann and Ganguly, 2003), and have been applied as geothermometers to many types of terrestrial rocks and chondrites (Wlotzka, 2005; Kessel et al., 2007). Unfortunately, the available calibrations yield widely differing temperatures for LAP 04840, from 850 to <400 °C.

Distribution of Fe and Mg between olivine and spinel has been used as a thermometer for many terrestrial lherzolites and several types of meteorites (Wlotzka, 2005; Kessel et al., 2007). When applied to the LAP 04840 mineral compositions, the calculated temperatures are clearly low: THERMOCALC gives ~470 °C, the Ballhaus et al. (1991) formulation gives ~560 °C, the Wlotzka (2005) calibration gives ~ 360 °C, and the QUILF program (Anderson et al., 1993) gives ~400 °C (although it does not treat Cr in the spinel). At these temperatures with sufficient water present, one would expect mineral assemblages with Fe–Mg amphibole rather than the olivine and orthopyroxene that are observed (Fig. 9; Evans et al., 2001). Perhaps the minerals totally exchanged the Mg/Fe during cooling, or the thermometer may be miscalibrated for metamorphic *T*.

The distribution of Fe and Mg between orthopyroxene and a spinel has been used as a thermometer for many terrestrial ultramafic rocks, but not extensively for meteorites. When applied to the LAP 04840 mineral compositions, the calculated temperatures are scattered. The THERMOCALC program returns a temperature of ~490 °C; the thermometric formulations of Liermann and Ganguly (2003, 2007) yield ~850 °C (estimated 2σ uncertainty ~50 °C),

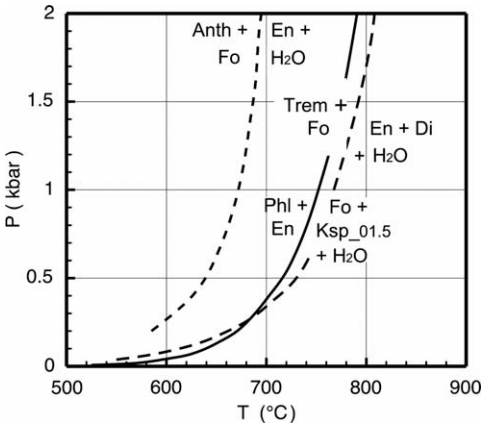

Fig. 9. Limiting equilibria for mineral assemblage and compositions in LAP 04840. Abbreviations are as follows: Anth, anthophyllite; Fo, forsterite; En, enstatite; Phl, phlogopite; Trem, tremolite; Di, diopside; Ksp, K-feldspar. As discussed in text, the P_{H_2O}–T conditions for equilibration of the silicate assemblage are constrained to be between the univariant reactions 4 (tremolite + forsterite = enstatite + diopside + H_2O; long-dashed line) and 2 (phlogopite + enstatite = forsterite + K-feldspar + H_2O; solid line) adjusted solid solutions in the minerals, and a plagioclase. These two reaction boundaries restrict $P_{H_2O} > 250$ bars. The inferred temperature of equilibration, $T = 670 \pm 60$ °C, from the amphibole–plagioclase thermometer of reaction 1 (Holland and Blundy, 1994), is consistent with this P_{H_2O}, and furthermore restricts $P_{H_2O} < 500$ bars.

and that of Sack and Ghiorso (1991), which is inherent in the MELTS thermochemical database (Ghiorso and Sack, 1995; Asimow and Ghiorso, 1998), also gives ~850 °C (estimated 2σ uncertainty ~50 °C).

5.1.4. Geothermometry summary

The mineral thermometry of LAP 04840 presents a confusing picture despite the chemical homogeneity of its minerals. We provisionally accept the amphibole-plagioclase temperature of 670 ± 60 °C as the result is close to the expected stability of the assemblage and compositional data in LAP 04840. Given their disparate results, Fe–Mg distributions between magnetite–olivine and magnetite–orthopyroxene seem unreliable for the LAP 04840 minerals. To justify the divergent results of the various thermometers, one may possibly invoke chemical re-equilibration of the magnetite in LAP 04840. If the magnetite had exchanged Fe and Mg with olivine at $T < 670$ °C, olivine–magnetite and orthopyroxene–magnetite geothermometers would give reset or spurious temperatures, reflecting in the best case the closure of their Fe–Mg exchanges. However, the composition of the olivine would change little in this re-equilibration because it is so much more abundant than magnetite (Table 1). Thus, results of mineral equilibria involving olivine will be affected only slightly, while those involving magnetite will be compromised.

5.2. Geobarometry

LAP 04840 contains minerals that can be used as sensors of water pressure (see below), but no assemblage that can be applied as a geobarometer at present (e.g., garnet–hornblende–plagioclase–quartz; e.g., Dale et al., 2000). The total Al content of hornblende has been used as a geobarometer in granitoids (Hammarstrom and Zen, 1986; Hollister et al., 1987; Johnson and Rutherford, 1989; Schmidt, 1992; Anderson and Smith, 1995), and could conceivably be applied here. However, application of the Al-in-hornblende barometer to LAP 04840 is problematic because the barometer has been evaluated only for granitoid to tonalitic rocks (Anderson and Smith, 1995), and because many factors besides pressure affect the Al content of amphibole (e.g., oxidation state, silica activity, partitioning of Al into other phases like biotite, substitution of Na, K, Fe^{3+}, and Ti in the hornblende, and compositions of melt and fluid phases). For instance, Shedlock and Essene (1979) showed that highly aluminous hornblende was stable at only ca. 1 kbar in magnesian skarns. Taking the Al content of LAP 04840 magnesiohornblende at face value in the Anderson and Smith (1995) formulation suggests a pressure of ~2.5 kbar; in light of the many factors that affect the total Al content of hornblende, this result has limited significance.

5.3. H_2O pressure

The mineral assemblage in LAP 04840 provides an unprecedented opportunity to constrain the partial pressure of water during metamorphism in a chondritic asteroid. We calculated P_{H_2O} from the locations of univariant reactions, using the computer program package THERMOCALC (Powell and Holland, 1988; Holland and Powell, 1990), as described above.

The mineral assemblage in LAP 04840 permits one chemical reaction that may directly constrain P_{H_2O} at peak metamorphism as a function of temperature, and several that act as upper or lower limits to that P_{H_2O}. The constraining reaction comes from the mineral assemblage phlogopite + orthopyroxene + olivine + albite:

$$\text{phlogopite} + \text{enstatite} = \text{forsterite} + \text{K} - \text{feldspar} + \text{H}_2\text{O}$$
$$KMg_3AlSi_3O_{10}(OH)_2 + 3MgSiO_3 = 3Mg_2SiO_4 + KAlSi_3O_8 + H_2O. \quad (2)$$

Other reactions limit the peak metamorphic P_{H_2O}, as the LAP 04840 mineral assemblage lacks a phase on either high- or low-T sides of the reactions. LAP 04840 lacks Fe–Mg amphibole, so that the reaction

$$\text{anthophyllite} + \text{forsterite} = \text{enstatite} + \text{H}_2\text{O}$$
$$Mg_7Si_8O_{22}(OH)_2 + Mg_2SiO_4 = 9MgSiO_3 + H_2O. \quad (3)$$

forms a low T, high P_{H_2O} limit to metamorphic conditions. On the other hand, LAP 04840 lacks augite, so this reaction

$$\text{tremolite} + \text{forsterite} = \text{enstatite} + \text{diopside} + \text{H}_2\text{O}$$
$$2Ca_2Mg_5Si_8O_{22}(OH)_2 + 2Mg_2SiO_4 = 10MgSiO_3 + 4CaMgSi_2O_6 + 2H_2O \quad (4)$$

limits peak metamorphic conditions on the high T, low P_{H_2O} side. (The reaction tremolite + phlogopite = enstatite + diopside + K-feldspar + H_2O (3 $Ca_2Mg_5Si_8O_{22}(OH)_2 + KMg_3AlSi_3O_{10}(OH)_2 = 12MgSiO_3 + 6CaMgSi_2O_6 + KAlSi_3O_8 + 4H_2O$ is always at higher T than

reaction 4 for the LAP 04840 assemblage, and so provides no additional constraints on P_{H_2O}.)

To locate these equilibria for the peak metamorphism of LAP 04840 (Fig. 9), the activities of chemical components in the minerals (Tables 4 and 5) were calculated with the THERMOCALC accessory program 'AX' (Powell and Holland, 2001), with two exceptions. For the albite composition of LAP 04840, 'AX' does not return an activity of $KAlSi_3O_8$ component; instead, it was calculated from the parameterization of Holland and Powell (2003) to be 0.139–0.246 at 670 °C (high and low K analyses). These values are nearly identical to those from the Elkins and Grove (1990) parameterization. The activity calculation is probably the most uncertain here, as the albite contains only 0.25–0.4% K_2O (1.6–3% $KAlSi_3O_8$), which significantly affects the activity of $KAlSi_3O_8$ in the feldspar (Elkins and Grove, 1990; Holland and Powell, 2003). Thus, we calculate the positions of reaction 2 for both K_2O abundances.

To apply the locations of reactions 3 and 4, limiting reactions that involve phases not present in LAP 04840, we calculated fictive mineral compositions constrained as much as possible by real mineral compositions. For the fictive composition of Mg–Fe–amphibole in reaction 3, a composition was calculated that would have been in Fe/Mg equilibrium with the LAP olivine (Frost, 1975). For the fictive augite in reaction 4, compositions were calculated that would have been in Fe–Mg equilibrium with the LAP 04840 orthopyroxene (Johnson and Essene, 1982) and would have a Ca content so that the augite lies on the augite–pigeonite solvus for the given T (Lindsley and Anderson, 1983).

The resultant reaction locations, calculated for the real and fictive mineral compositions, are permissive of a small wedge of T–P_{H_2O} space for the peak metamorphic conditions of LAP 04840 (Fig. 9). The trace of the phlogopite + enstatite breakdown reaction (2) is shown in Fig. 9 for 1.5% molar $KAlSi_3O_8$ component (0.25% K_2O in the albite). If the activity models are accurate and precise, the actual peak T–P_{H_2O} must lie between these curves. In addition, reaction 4 (the breakdown of amphibole + forsterite to enstatite + diopside + H_2O) provides a stricter limit on the high T side (Fig. 9), so that the peak metamorphic T–P_{H_2O} must fall between its location and that of reaction 3 with 1.5% molar $KAlSi_3O_8$ in albite. These two curves are separated by <20 °C at $P_{H_2O} < 2$ kbar; they cross at 0.25 kbar, which is the lowest pressure at which the LAP 04840 mineral assemblage (phlogopite + enstatite + amphibole) could be stable, and thus the lowest possible pressure of peak metamorphism. The nominal equilibration temperature from hornblende–plagioclase thermometry, 670 ± 60 °C, includes the lower-temperature end of this permitted wedge; the upper limit of this temperature range would limit $P_{H_2O} = P_{total}$ to less than ~500 bars.

5.4. Oxygen fugacity

The R chondrites (including LAP 04840) are very oxidized compared to other chondrites (Brearley and Jones, 1998); qualitative measures of their oxidation state include a lack of Fe–Ni metal, high Ni contents in the olivine (LAP 04840 ~0.4 wt%) (O'Neill and Wall, 1987; Ehlers et al., 1992), and presence of a spinel with significant ferric iron (magnetite component). Similarly, the Mössbauer data suggests a high oxidation state as evidenced by the abundant ferric iron in the silicate minerals: olivine has Fe^{3+}/Fe_{tot} of ~5%, biotite has Fe^{3+}/Fe_{tot} of ~65%, and the hornblende has Fe^{3+}/Fe_{tot} of ~80% Fe^{3+} (Tables 2 and 4). These Fe^{3+}/Fe_{tot} values are similar to those in metasomatized mantle xenoliths on Earth, which are inferred to have formed at high oxidation states near the quartz–fayalite–magnetite (QFM) oxygen buffer (McGuire et al., 1991).

Mineral equilibria allow a quantitative estimate of the oxygen fugacity, f_{O_2}, during the metamorphism of LAP 04840, although the composition of the magnetite was inferred above to have been affected by back-reaction. Oxygen fugacity can be calculated from the compositions of minerals in the assemblage olivine + orthopyroxene + spinel (Table 4) via the equilibrium

$$\text{fayalite} + O_2 = \text{ferrosilite} + \text{magnetite}$$
$$6Fe_2SiO_4 + O_2 = 3Fe_2Si_2O_3 + 2Fe_3O_4. \quad (5)$$

Using THERMOCALC, the mineral compositions of LAP 04840 are inferred to have been in equilibrium at f_{O_2} values slightly above those of the QFM buffer, averaging ~ΔQFM + 0.3 log units ($\log_{10} f_{O_2}$) at temperatures between 550 and ~800 °C. Similar results are obtained from the empirical oxybarometer of Wood (1991), which returns an f_{O_2} of ΔQFM + 0.7 ± 0.5 log units for 670 °C (from the amphibole–plagioclase geothermometer). These two independent determinations of f_{O_2} are within uncertainty, and also within uncertainty of the independent determination by Righter and Neff (2007).

These calculations depend on the composition of the chromian magnetite in LAP 04840; we inferred that the compositions of the magnetite and olivine were reset at temperatures below that of peak metamorphism. If so, the oxygen fugacities calculated here must be considered semi-quantitative, but are likely close to the real fugacities using the Δ format (i.e., ΔQFM + 0.5). The calculations here are likely correct for the temperature of olivine–spinel Fe–Mg equilibration (roughly 500 °C), and the THERMOCALC output shows that f_{O_2} for these mineral compositions is only a weak function of temperature.

5.5. Other volatile fugacities

The fugacities of C-bearing gas species cannot be determined because LAP 04840 lacks C-bearing minerals, neither carbonates nor graphite. The absence of magnesite indicates that $P_{CO_2} < 6.2$ kbar (for $T < 700$ °C), as constrained by the reaction

$$\text{enstatite} + 2\text{magnesite} = 2\text{forsterite} + 2CO_2$$
$$2MgSiO_3 + 2MgCO_3 = 2Mg_2SiO_4 + 2CO_2, \quad (6)$$

using the analyzed compositions of olivine and orthopyroxene, and a fictive carbonate in Fe–Mg equilibrium with the olivine (Dalton and Wood, 1993). This limiting constraint is not useful in the context of asteroid metamorphism.

The fugacity of sulfur gas, f_{S_2}, during the metamorphism of LAP 04840 can be calculated from the equilibrium

$$\text{pyrrhotite} + O_2 = \text{magnetite} + S_2$$
$$6FeS + 4O_2 = 2Fe_3O_4 + 3S_2, \quad (7)$$

using mineral compositions in LAP 04840 and the calculated f_{O_2}. The f_{S_2} calculation was done manually with Gibbs free energy data for Fe_3O_4 and FeS from Robie et al. (1978), as the THERMOCALC database does not include sulfides. The activity of Fe_3O_4 in the chromian magnetite in the spinel structure oxide was as calculated by the 'AX' program, and FeS activity was calculated from the formulation of Toulmin and Barton (1964). At an f_{O_2} of ~QFM + 0.5 log units, this reaction implies a $\log f_{S_2}$ value of ~ −10, two log units above that of the iron–troilite buffer reaction, and 9 log units below that of the pyrrhotite–pyrite buffer reaction. Of course, neither of these buffer reactions could be achieved in LAP 04840 at peak metamorphism because f_{O_2} is too high for iron metal to be present, and the f_{S_2} is too low for pyrite to be stable.

Fugacities of the halogens Cl and F can be constrained by mineral reactions involving halogen-bearing biotite and apatite. Halogen contents of metamorphic biotites are functions of the fugacities of HCl and HF, and other parameters including temperature and Mg/Fe ratios (Munoz and Ludington, 1974; Munoz, 1984, 1992; Sisson, 1987; Zhu and Sverjensky, 1992). Using the phlogopite composition in Table 4 and the equilibrium metamorphic temperature of 670 °C, we applied the formulations of Munoz (1992) to calculate average $\log(f_{HF}/f_{H_2O}) = -5.8$, $\log(f_{HCl}/f_{H_2O}) = -3.3$, and $\log(f_{HCl}/f_{HF}) = -2.6$. Halogen fugacities calculated using the apatite composition and partitioning data (Zhu and Sverjensky, 1992) show similar values: $\log(f_{HF}/f_{H_2O}) = -4.8$, $\log(f_{HCl}/f_{H_2O}) = -1.9$, and $\log(f_{HCl}/f_{HF}) = -2.8$). These values suggest that if a distinct volatile phase was present, it was dilute with Cl in significant excess over F.

5.6. Petrologic grade

LAP 04840 was originally classified as R6 (Satterwhite and Righter, 2006). Petrologic grade 6 implies extensive textural equilibration, to the point that chondrule textures become obscure (van Schmus and Wood, 1967), but chondrule boundaries of chondrules in LAP 04840 are distinct at scales of 10–20 μm (Fig. 2B and C), suggesting a grade of 4–5 (van Schmus and Wood, 1967). On the other hand, mineral compositions in LAP 04840 are nearly homogeneous across and among grains (Figs. 5–7), w hich is inconsistent with petrologic grade 4 (van Schmus and Wood, 1967). Thus, LAP 04840 should be classified as grade 5, as an R5 chondrite.

6. INTERPRETATION

The important issues raised by LAP 04840 center on its OH-bearing minerals such as ferri-magnesiohornblende and phlogophite, which represent a unique assemblage among chondrites, and nearly unique among meteorites (the other instance being the Martian meteorite Chassigny: Watson et al., 1994). The texture of LAP 04840, its bulk composition, and the compositions of its anhydrous minerals are unremarkable for a chondrite (Figs. 1, 2, 5, and Tables 4 and 5), as are its peak temperature of metamorphism (e.g., Wlotzka, 2005; Kessel et al., 2007), and oxidation state (Kallemeyn et al., 1996). However, the abundant OH-bearing minerals in LAP 04840 raise two general questions: how did the hydrogen enter the meteorite, i.e. the physical and chemical conditions of its hydrogenation/hydration; and the original source of the hydrogen.

This discussion implicitly assumes that LAP 04840 was modified from a precursor, unmetamorphosed, anhydrous R chondrite. This inference seems reasonable in light of the similarities between LAP 04840 and 'normal' R chondrites (bulk composition, Table 3; mineral compositions, Table 4; O isotope composition, Table 7; and oxidation state), and is similar to the longstanding hypothesis that high-grade ordinary chondrites (groups H, L, and LL; grades 4–6) are metamorphosed equivalents of unequilibrated ordinary chondrites (e.g., Brearley and Jones, 1998).

6.1. Depth of metamorphism

The range of P_{H_2O} during metamorphism of LAP 04840, 250–500 bars, provides a significant constraint on the depth of metamorphism, and thus its geological setting and tectonics. The calculated P_{H_2O} is low, and on Earth would imply either shallow depths (e.g., <1.5 km for $P_{H_2O} = P_{total}$), or significantly reduced activity of water (e.g., $P_{H_2O} \ll P_{total}$). However, the depth would be much greater on an asteroid, because of its smaller size and lower gravity.

To illustrate the depth constraint provided by the calculated P_{H_2O}, Fig. 10 shows the depths required to achieve lithostatic pressures of 250 and 500 bars in homogeneous asteroids ($\sigma = 3.0$ g/cm^3) of various radii. Significant depths are required from >25 km depth in an asteroid of 50 km radius, to >2 km for a parent body of 800 km radius. For reference, the largest known asteroid, 1 Ceres, has a radius of 460 km; the parent asteroids of ordinary chondrite meteor-

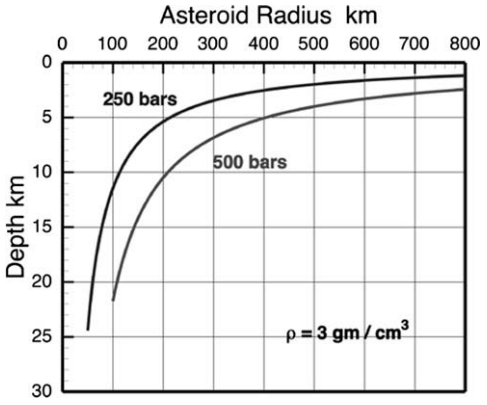

Fig. 10. Semi-quantitative pressure-depth relationship for LAP 04840. The water pressure during its metamorphism is calculated to be between 250 and 500 bars (Fig. 9); the labeled curves here show the depth within an asteroid of a given radius at which that pressure would be achieved, assuming that the asteroid is homogeneous with a density of 3 g/cm^3. Depths from this graph are considered minima because the upper few kilometers of a real asteroid would likely be an impact regolith, and thus porous and of lower density.

ites are inferred to be ~50–100 km in radius (Bennett and McSween, 1996; McSween et al., 2002).

The depths from Fig. 10 must be considered minima from two reasons: porosity and fluid diluents. A real asteroid would not be of homogeneous density, but would have a significant thickness of porous regolith near its surface. Porous regolith is less dense than solid rock, meaning that the depth required to achieve a given pressure are greater than in Fig. 10. Similarly, Fig. 10 shows lithostatic pressure—the pressure that the solid grains exert on each other. The pressure experienced by a fluid, between the solid grains, can be significantly less than lithostatic if the asteroid has a connected permeability (e.g., if it is a loose rubble pile or significantly fractured). Significant connected permeability would also mean that depths inferred from Fig. 10 are minima. Finally, if the fluid were not pure water but were mixed with other constituents, the H_2O activity would be less than unity, and the depths inferred from Fig. 10 would again be minima.

6.2. Hydration/hydrogenation

If LAP 04840 formed by metamorphism of a typical anhydrous R chondrite, then its relatively abundant H (or H_2O) must have entered this protolith from elsewhere. First, it seems reasonable that a distinct fluid phase was involved. Without a fluid phase, H and/or OH could have entered the protolith only by solid-state and grain-boundary diffusion, which are slow relative to fluid advection (Baumgartner and Valley, 2001). Second, it seems likely that the metamorphic fluid phase was relatively oxidized, i.e. mostly H_2O and CO_2. If the fluid had been rich in reduced species like H_2 and CH_4, it would have altered the protolith R chondrite from its original high oxidation state to be more reduced. LAP 04840 is not reduced compared to other R chondrites, so it seems likely that the metamorphic fluid was relatively oxidized (consistent with f_{O_2} of $\sim\Delta$QFM + 0.5 log units), and thus probably dominated by H_2O and CO_2. The P_{H_2O} during metamorphism was between 250 and 500 bars, as calculated above, although the partial pressure of CO_2 is nearly unconstrained.

Third, it is important to know if the fluid that hydrated/hydrogenated LAP 04840 caused any additional metasomatism, i.e., whether elements besides H or H_2O were transported into or out of the rock. We have no evidence of such metasomatism, because the calculated bulk composition of LAP 04840 is nearly identical to those of anhydrous R chondrites (Table 3), and the difference between LAP 04840 and the other R chondrites is within the variability seen among same-type chondrites (e.g., see Table 2 of Jarosewich, 2006). Similarly, the oxygen isotope composition of LAP 04840 is consistent with those of other R chondrites (see above; Greenwood et al., 2000). This absence of metasomatism in the transition from an R chondrite protolith to the hydrated LAP 04840 suggests two possible explanations. The fluid could have been nearly pure H_2O (with or without inert diluents like CO_2), and so entered the protolith carrying no foreign chemical components. However, such a fluid would have dissolved something from the LAP 04840 protolith; if any of the fluid passed through the rock LAP 04840 should be depleted in these soluble components. On the other hand, if LAP 04840 had been perfused with a water-rich fluid that had already equilibrated with other masses of R chondritic rock, the fluid might leave little trace behind (besides its water). Such a fluid, by the time it encountered LAP 04840, would have already dissolved what it could from the other R chondrite material, so it would not dissolve or deposit much (besides water) as it passed into and through LAP 04840.

6.3. Timing and reaction of hydration

If LAP 04840 developed from an initially anhydrous R chondrite protolith, it is important to understand when the hydrogen (or water) entered the rock. The protolith could have been hydrated before metamorphism, in low-temperature aqueous alteration, to form minerals like clays, serpentines, epidote, zeolites, etc., the present magnesiohornblende and phlogopite would have formed after those minerals dehydrated. On the other hand, the protolith could have been hydrated near the peak of metamorphism.

Other chondrites exhibit a range in their degrees of aqueous alteration that offer some clues to what one might expect if LAP 04840 had been hydrated prior to metamorphism. Carbonaceous chondrites show the most extensive aqueous alterations, and largest range of alteration features. CI chondrites are essentially completely altered, and therefore of little relevance to this discussion because relict chondrules remain in LAP 04840. CM and CR chondrites exhibit a wide range of degrees of alteration (McSween, 1979; Weisberg et al., 1993; Browning et al., 1996; Weisberg and Prinz, 2000; Abreu and Brearley, 2006; Rubin et al., 2007; Weisberg and Huber, 2007; Bunch et al., 2008). In the least altered chondrites, the alteration is confined to the matrix. With progressive alteration, the chondrule glass is first attacked, followed by often pseudomorphic replacement of the chondrule olivine and low-Ca pyroxene phenocrysts. Carbonates, primarily calcite and dolomite, appear to be ubiquitous products of aqueous alteration in CIs, CMs, CRs and the unique chondrite Tagish Lake. In the Bali-like subgroup of oxidized CVs, evidence for alteration is largely confined to the matrix and the outer margins of chondrules (Krot et al., 1995, 1998). Alteration products include the phyllosilicates saponite and phlogopite, and anhydrous minerals such as fayalite and Ca–Fe-rich pyroxenes. Krot et al. (1998) inferred alteration temperatures of <300 °C for these meteorites. For the Allende-like oxidized CVs, alteration seems to have occurred at higher temperatures. Phyllosilicates are rare in these meteorites, with the major alteration minerals being anhydrous fayalitic olivine, nepheline, sodalite, and Ca–Fe-rich pyroxene. The GRO95571 meteorite, a CR1, is particularly relevant here as it is composed almost entirely of phyllosilicates, in near-perfect replacements and pseudomorphs of chondrule textures (Weisberg and Huber, 2007).

A few carbonaceous chondrites (CMs) have been strongly metamorphosed following their hydration, probably as a result of shock. They show clear evidence of devol-

atilization of phyllosilicates and carbonates (Tonui et al., 2002; Nakamura, 2005).

Ordinary (non-carbonaceous) chondrites show a similar pattern of alteration effects. Semarkona (LL3.0) is the most extensively altered ordinary chondrite (Hutchison et al., 1987; Alexander et al., 1989). Semarkona's matrix is almost completely altered and contains carbonates (Hutchison et al., 1987; Alexander et al., 1989), and glass in some of its chondrules has been partially hydrated (Grossman et al., 2000, 2002). Many excentroradial chondrules in ordinary chondrites (notably Semarkona) have distinctive bleached outer regions, where felsic glass has been leached away or replaced by clay minerals (Grossman et al., 2000). Hence, Grossman et al. (2000) proposed that all ordinary chondrites underwent at least limited aqueous alteration prior to metamorphism and dehydration; however, this alteration was apparently restricted to leaching and alteration of matrix materials and chondrule glasses.

Most mineral textures in LAP 04840 are not consistent with this style of low-temperature alteration, and so suggest that hydration/hydrogenation at high temperature is most likely. The presence of amphibole in place of mesostasis in some chondrules (Fig. 2B) is a reasonable product of metamorphism of hydrous mesostasis glass or of clay and serpentines after mesostasis glass. However, the nearly random distribution of amphibole in the meteorite in both matrix and most chondrules (Figs. 1A and, 2A and D) suggest widespread extensive alteration unlike that of ordinary chondrites. Had alteration been so widespread and pervasive, it seems unlikely that the large olivine and orthopyroxene crystals of chondrules would remain unscathed, but would have been replaced by aggregates of minerals characteristic of lower temperatures, including: clays, serpentine minerals, Fe–Mg amphibole, albite, epidote, prehnite, pumpellyite, and carbonates (Spear, 1993). When heated to ~700 °C, as was LAP 04840, these minerals would have dehydrated to form olivine and orthopyroxene again, but the new mineral grains would not re-create the shapes and sizes of the original chondrule olivine and pyroxene. Rather, the new texture would likely show aggregates of small grains pseudomorphing the shapes of the original grains. Because LAP 04840 does not show this texture (Fig. 2A and D), it seems likely that hydration/hydrogenation occurred at P_{H_2O}–T conditions where olivine and orthopyroxene were stable, i.e. above the reaction anthophyllite + forsterite = enstatite + H_2O (Fig. 9).

Finally, it seems likely that the amphibole in LAP 04840 formed at the expense of augite in the protolith. Augite is the dominant pyroxene in metamorphosed R chondrite materials, up to 15% by volume (Kallemeyn et al., 1996; Berlin and Stöffler, 2004), and carries the bulk of their calcium. On the other hand, LAP 04840 has no augite, and most of its Ca is sited in the ~ 15% magnesiohornblende (Tables 1 and 5). So, it seems likely that the hornblende-forming reaction involved augite, e.g.,

$$\text{augite} + \text{plagioclase} + \text{orthopyroxene} + \text{olivine} + H_2O = \text{hornblende} \quad (8)$$

and ceased when the augite was completely consumed. This reaction is the reverse of the hornblende-out reaction in the transition from amphibolites to mafic granulites in the absence of quartz (e.g., Spear, 1981, 1993), and is akin to amphibole forming reactions during retrograde metamorphism of mafic granulites on Earth.

6.4. Origin of D-enriched Hydrogen

The source of the hydrogen in LAP 04840 is a crucial constraint on the meteorite's origin and history; its D/H ratio is quite unusual, excluding most simple and obvious scenarios, and permitting only a few (potentially problematic) ones. The isotopic composition of hydrogen in LAP 04840 hornblende, which we take as that of the whole rock, is $\delta D = +3660 \pm 75‰$ (Table 6). This value is much higher than those of most known H reservoirs in the early solar system. So, one can consider two (rather arbitrary) divisions in looking at the origin of H in LAP 04840: unusual sources, and unusual processes.

6.4.1. D-Rich source

Few H reservoirs in the early solar system have D/H ratios that are high enough to represent sources for the H in LAP 04840—typical δD values include: protosolar disk material, ~−850‰; Earth, near 0‰; bulk carbonaceous chondrites, to ~ +1000‰; and cometary water ~+1000‰ (McKeegan and Leshin, 2001; Robert, 2002; Drake, 2005; Ohtani, 2005). In primitive solar system materials, there appear to be two hydrogen reservoirs with sufficiently high δD values. First, insoluble organic matter (IOM) in the matrices of some primitive chondrites have bulk H/C ratios (atomic) of ~0.2 to 0.7 and δD values of their components range from ~+2500‰ to +5500‰ (varying by meteorite class: Robert and Epstein, 1982; Yang and Epstein, 1984; Alexander et al., 2007a; Remusat et al., 2006). Meteoritic IOM and interplanetary dust particles have isotopic 'hot spots' with δD up to +50,000‰ (Messenger, 2002; Keller et al., 2004; Busemann et al., 2006; Alexander et al., 2007b), but it seems unlikely that the H from these hotspots could be isolated from the H in the bulk of the organics. Second, phyllosilicate minerals and glasses in the LL3.0 chondrite Semarkona (the least metamorphosed known) contain H with δD values of +3300 to +4600‰ (McNaughton et al., 1982; Deloule and Robert, 1995; Grossman et al., 2000, 2002). However, Semarkona seems unique among chondrites in having such deuterated water.

Whilst one cannot exclude the possibility that LAP 04840 represents a previously unrecognized H reservoir of the early solar system, of the known high δD reservoirs, meteoritic IOM is the most abundant and widespread, and so is the most reasonable known source of the H in LAP 04840. IOM has not yet been reported in any R chondrites. In the lowest petrologic type chondrites, IOM is present in their matrices at relatively constant abundances (Alexander et al., 1998, 2007a). However, it is destroyed by metamorphism. In OCs, IOM has all but disappeared by petrologic type 3.6–3.7, which corresponds to peak temperatures <~400 °C (Alexander et al., 1998, 2007a; Busemann et al., 2007; H3.7 and L3.7 chondrites experienced peak temperatures of ~620–680 °C; Wlotzka, 2005); little R chondrite material is so lightly metamorphosed (Bischoff,

2000; Imae and Zolensky, 2003). Oxidation is probably the principal mechanism of IOM destruction in the OCs. R chondrites are even more oxidized (near the QFM buffer), and contain abundant ferrous and ferric iron (Table 3) which could act as oxidants for IOM. Hence, the fact IOM has not been reported (to our knowledge) in R chondrites can be simply ascribed to their relatively high metamorphic grades.

In terms of O isotopes and matrix abundance, R chondrites most closely resemble the OCs. Upon oxidation, the IOM in Semarkona could generate ~0.13 wt% water and about 10 times as much by weight of CO_2, but Semarkona IOM may have already lost ~30% of its H as a result of parent body processes (Alexander et al., 2007a). There is no sign of this CO_2 in LAP 04840, i.e., no carbonate minerals are present. The absence of carbonate minerals in the mineral assemblage of LAP 04840, as calculated above, implies that $P_{CO_2} < 6.2$ kbar, a rather high limit in relation to P_{H_2O} and possible sizes of asteroids (Fig. 10).

6.4.2. Enrichment mechanisms

On the other hand, the high δD in LAP 04840 could have arisen by fractionation and D-enrichment from a more normal source of H (i.e., δD of ~0‰ to +1000‰). Two processes seem capable of producing such extreme fractionations: atmospheric escape, and fractionation of H_2 from water.

The atmospheres of Mars and Venus have high δD, ~+4400 and ~+150,000, respectively, which are ascribed to fractionation of H from D in the upper atmosphere, and loss of the higher-flying H to space (Kasting and Pollack, 1983). This process seems unlikely for a chondritic asteroid source for LAP 04840, which should have had only the most tenuous atmosphere. One cannot exclude the possibility that the parent planetesimal of LAP 04840 was large enough to maintain a significant atmosphere for some time that it could have evolved to a high D/H value. If so, the parent planetesimal must have had some mechanism for transferring D-rich water from the atmosphere to the planetesimal surface (i.e., precipitation), and thence into the metamorphic environment of LAP 04840 (i.e., an active groundwater system). This scenario seems to imply a Mars-sized planet, for which there is no other evidence (note that O isotope ratios are inconsistent with a Martian origin for LAP 04840).

Another process that can produce high δD-water is low-temperature equilibration with H_2 gas; D is strongly fractionated into liquid water compared to H_2 gas (0–200 °C; Rolston et al., 1976). Two pathways have been suggested for production of H_2 from water in planetary interiors: reduction and radiolysis. Reduction would include reaction of water with iron metal to yield ferrous iron (in silicates and/or oxides) and H_2, and reaction of water with ferrous iron to yield H_2 and ferric iron (in minerals like magnetite; Dreibus and Wänke, 1987; Elkins-Tanton and Seager, 2007). Radiolysis is decomposition of water under the action of ionizing radiation, and has been suggested as a potential source of H_2 in the Earth's subsurface (Lin et al., 2005). Radiolysis could be very significant in an early planetesimal, with its primordial abundances of now-extinct radionuclides like ^{26}Al.

Neither reduction nor radiolysis could produce water with δD = +3700‰ at equilibrium—though large, the equilibrium fractionation factor is not that large (Rolston et al., 1976). However, H_2 could escape readily from such water, either by degassing or by incorporation into metal, which permits the possibility of continuous (Rayleigh) fractionation. With such a large fractionation factor, Rayleigh distillation could readily produce water, in moderate abundance, with high δD values. This scenario should be explored further.

6.5. Mechanism of hydration

Beyond the obscure origin of D-enriched water in LAP 04840, it is equally obscure how the water came to enter LAP 04840, but not other R chondrites, and produce its magnesiohornblende and phlogopite. The fundamental problem (as described above) is that LAP 04840 was hydrated while hot. In simple 'onion-skin' metamorphism of an asteroid, heat is produced mostly by radioactive decay (especially of short-lived nuclides) and the temperature increases monotonically with depth (McSween et al., 2002). As a result of increasing temperature, the asteroid's IOM and rocks become progressively equilibrated, oxidized, and dehydrated with depth. Consequently, this destruction of IOM would leave no source of water for LAP 04840. Similarly, if true, this scenario would suggest that water-bearing metamorphosed R chondrites (and others) should be abundant, rather than known only as a single example.

So, the origin of LAP 04840 must involve an unusual metamorphic scenario, in which hot dry rock comes to lie above or adjacent to cooler, hydrogen-bearing rock. On Earth, for instance, this scenario can be realized above subduction zones or major thrust faults. On a primitive asteroid, two other scenarios are possible and are much more likely: impact heating, and disruption/reassembly.

First, a large impact event would produce a zone of heated rock near the asteroidal surface, and perhaps a sheet of impact melt in the resultant crater (e.g., Melosh, 1989). These hot zones would sit above cooler, and potentially H-bearing, rock, creating a system in which rock heated by the impact could be hydrated by water from beneath (e.g., Abramov and Kring, 2005; Naumov, 2005). However, this scenario is problematic because: (1) hydrothermal alteration around impact craters is most pervasive at lower temperatures (<300 °C) because hotter rock supports few fractures (Abramov and Kring, 2005) and (2) very little rock around an impact crater is as hot as 700 °C (as LAP 04840 was) without being either impact melt or heavily deformed central peak/ring material (as LAP 04840 is not).

Another possible mechanism is asteroid disruption by a large impactor, followed by gravitational re-assembly and consolidation of the fragments (e.g., Richardson et al., 2002; Scott and Wilson, 2005). One could imagine cool, hydrogen-bearing rock from near the surface of either asteroid (target or impactor) being buried deeply during re-assembly, surrounded by hot rock from the interiors of the original asteroids (Grimm, 1985). Hydrogen or water released by metamorphism of the surface rock would then

react with hotter adjacent asteroid fragments to produce high-temperature hydrous minerals like magnesiohornblende and phlogopite.

7. CONCLUSIONS

The R chondrite LAP 04840 is classified as an R5 chondrite (shock stage S2) and consists of olivine, orthopyroxene, plagioclase, magnesiohornblende, pyrrhotite, pentlandite, magnetite, and minor accessory phases (phlogopite, apatite). This meteorite is unique among meteoritic material as it contains extraterrestrial OH-bearing minerals (magnesiohornblende and phlogopite). With the exception of these OH-bearing phases, this meteorite is similar to other known R chondrites suggesting metamorphism is responsible for the mineralogy of LAP 04840. The metamorphic conditions necessary to result in the observed phase assemblage and textures have been determined to be: $T = 670 \pm 60$ °C and P_{H_2O} between 250 and 500 bars, with volatile fugacities of $f_{O_2} = \mathrm{QFM} + 0.5$, $\log f_{S_2} = -10$, $\log(f_{HF}/f_{H_2O}) = -5.8$, $\log(f_{HCl}/f_{H_2O}) = -3.3$, and $\log(f_{HF}/f_{HCl}) = -2.6$. Comparison with other R chondrite compositions, as well as the mineralogy, suggest the LAP 04840 was hydrated at high temperature through introduction of an oxidized fluid phase. The large D enrichments of the fluid phase as measured in the amphibole are consistent with oxidation of insoluble organic matter through heating. However, the lack of widespread fluid-driven metamorphism within the known R chondrite samples implies that LAP 04840 may have been produced through a unique series of events, potentially by collision.

ACKNOWLEDGMENTS

The are grateful to the ANSMET program, the NASA Antarctic Meteorite Curator, and the Meteorite Working Group for allowing us access to this unique meteorite. Craig Schwandt and Anne Peslier (JSC/Jacobs Sverdrup) assisted with EMP analyses, and Matt Manon (U. Michigan) aided with thermochemical calculations. This work has benefited from discussions with J. Grossman, A. Rubin, G. Rossman, and T. McCoy. Critical reviews by A. Bischoff, E. Deloule, and A. Rubin are gratefully acknowledged. A.H.T. acknowledges support from the NASA Astrobiology Institute node at the NASA Ames Research Center, and NASA grant NNG06GH29G. C.M.O'D.A. was partially funded by NASA Astrobiology Institute node at the Carnegie Institution of Washington. Part of this work was done while M.C.M. was a Urey Post-Doctoral fellow at the LPI. Lunar and Planetary Institute Contribution #1419.

REFERENCES

Abramov O. and Kring D. A. (2005) Impact-induced hydrothermal activity on early Mars. *J. Geophys. Res.* **110**, E12S09. doi:10.1029/2005JE002453.

Abreu N. M. and Brearley A. J. (2006) Early Solar System processes recorded in the matrices of CR2 chondrites MET 00426 and QUE 99177. *Lunar Planet. Sci.* **XXXVII**, Lunar Planet. Inst., Houston. #2395 (abstr.).

Alexander C. M. O'D., Barber D. J. and Hutchison R. (1989) The microstructure of Semarkona and Bishunpur. *Geochim. Cosmochim. Acta* **53**, 3045–3057.

Alexander C. M. O'D., Russell S. S., Arden J. W., Ash R. D., Grady M. M. and Pillinger C. T. (1998) The origin of chondritic macromolecular organic matter: a carbon and nitrogen isotope study. *Meteorit. Planet. Sci.* **33**, 603–622.

Alexander C. M. O'D., Fogel M., Yabuta H. and Cody G. D. (2007a) The origin and evolution of chondrites recorded in the elemental and isotopic compositions of their macromolecular organic matter. *Geochim. Cosmochim. Acta* **71**, 4380–4403.

Alexander C. M. O'D., Boss A. P., Keller L. P., Nuth J. A. and Weinberger A. (2007b) Astronomical and meteoritic evidence for the nature of interstellar dust and its processing in protoplanetary disks. In *Protostars and Planets V* (eds. B. Reipurth, D. Jewitt and K. Keil). University of Arizona Press, Tucson, pp. 801–813.

Anderson J. L. and Smith D. R. (1995) The effects of temperature and f_{O_2} on the Al-in-hornblende barometer. *Am. Mineral.* **80**, 549–559.

Anderson D. J., Lindsley D. H. and Davidson P. M. (1993) QUILF: a Pascal program to assess equilibria among Fe–Mg–Mn–Ti oxides, pyroxenes, olivine, and quartz. *Comput. Geosci.* **19**, 1333–1350.

Asimow P. D. and Ghiorso M. S. (1998) Algorithmic modifications extending MELTS to calculate subsolidus phase relations. *Am. Mineral.* **83**, 1127–1131.

Ballhaus C., Berry R. F. and Green D. H. (1991) High pressure experimental calibration of the olivine–orthopyroxene–spinel oxygen barometer: implications for the oxidation state of the mantle. *Contrib. Mineral. Petrol.* **107**, 27–40.

Baumgartner L. P. and Valley J. W. (2001) Stable isotope transport and contact metamorphic fluid flow. *Rev. Mineral. Geochem.* **43**, 415–467.

Bennett . M. E. and McSween, Jr., H. Y. (1996) Revised model calculations for the thermal histories of ordinary chondrite parent bodies. *Meteorit. Planet. Sci.* **31**, 783–792.

Berlin J. and Stöffler D. (2004) Modification of the Van Schmus & Wood petrologic classification for lithic fragments in the chondritic breccia Rumuruti. *Lunar Planet. Sci.* **XXXV**, Lunar Planet. Inst., Houston. #1344 (abstr.).

Bibring J.-P.the OMEGA team (2006) Global mineralogical and aqueous Mars history derived from OMEGA/Mars Express data. *Science* **312**, 400–404.

Bischoff A. (1998a) Aqueous alteration of carbonaceous chondrites: evidence for preaccretionary alteration. A review. *Meteorit. Planet. Sci.* **33**, 1113–1122.

Bischoff A. (2000) Mineralogical characterization of primitive, type-3 lithologies in Rumuruti chondrites. *Meteorit. Planet. Sci.* **35**, 699–706.

Bischoff A., Geiger T., Palme H., Spettel B., Schultz L., Scherer P., Loeken T., Bland P., Clayton R. N., Mayeda T. K., Herpers U., Meltzow B., Michel R. and Dittrich-Hannen B. (1994) Acfer 217—a new member of the Rumuruti chondrite group (R). *Meteoritics* **29**, 264–274.

Bischoff A., Weber D., Bartoschewitz R., Clayton R. N., Mayeda T. K., Schultz L., Spettel B. and Weber H. W. (1998b) Characterization of the Rumuruti chondrite regolith breccia Hughes 030 (R3–6) and implications for the occurrence of unequilibrated lithologies on the R chondrite parent body. *Meteorit. Planet. Sci.* **33**, A15 (abstr.).

Boynton W. V. et al. (2002) Distribution of hydrogen in the near surface of Mars: evidence for subsurface ice deposits. *Science* **297**, 81–85.

Brearley A. J. and Jones R. H. (1998) Chondritic meteorites. In *Planetary Materials*, vol. 36 (ed. J. J. Papike). Mineralogical Society of America, Washington, DC.

Browning L. B., McSween, Jr., H. Y. and Zolensky M. E. (1996) Correlated alteration effects in CM carbonaceous chondrites. *Geochim. Cosmochim. Acta* **60**, 2621–2633.

Bunch T. E., Irving A. J., Wittke J. H., Rumble, III, D., Gellissen M. and Palme H. (2008) Evidence for pervasive metamorphism on the CR chondrite parent body from highly equilibrated CR6 chondrites Northwest Africa 2994 and Northwest Africa 3100. *Lunar Planet. Sci.* **XXXIX**, Lunar Planet. Inst., Houston. #1991 (abstr.).

Busemann H., Young A. F., Alexander C. M. O'D., Hoppe P., Mukhopadhyay S. and Nittlerm L. R. (2006) Interstellar chemistry recorded from primitive meteorites in organic matter. *Science* **314**, 727–730.

Busemann H., Alexander C. M. O'D. and Nittler L. R. (2007) Characterization of insoluble organic matter in primitive meteorites by microRaman spectroscopy. *Meteorit. Planet. Sci.* **42**, 1387–1416.

Carr M. H. (1996) *Water on Mars*. Oxford University Press, New York.

Christensen P. R. et al. (2004) Mineralogy at Meridiani Planum from the Mini-TES experiment on the Opportunity Rover. *Science* **306**, 1733–1739.

Cosca M. A., Essene E. J. and Bowman J. R. (1991) Complete chemical analyses of metamorphic hornblendes: implications for normalizations, calculated H_2O activities, and thermobarometry. *Contrib. Mineral. Petrol.* **108**, 472–484.

Dale J., Holland T. and Powell R. (2000) Hornblende–garnet–plagioclase thermobarometry: a natural assemblage calibration of the thermodynamics of hornblende. *Contrib. Mineral. Petrol.* **140**, 353–362.

Dalton J. A. and Wood B. J. (1993) The partitioning of Fe and Mg between olivine and carbonate and the stability of carbonate under mantle conditions. *Contrib. Mineral. Petrol.* **114**, 501–509.

Davies J. K., Roush T. L., Cruikshank D. P., Bartholomew M. J., Geballe T. R., Owen T. and deBergh C. (1997) The detection of water ice in comet Hale-Bopp. *Icarus* **127**, 238–245.

Deer W. A., Howie R. A. and Zussman J. (1983) *An Introduction to the Rock-Forming Minerals*. Longman Group, Ltd., Essex, England.

Deloule E. and Robert F. (1995) Interstellar water in meteorites?. *Geochim. Cosmochim. Acta* **59** 695–706.

Donahue T. M., Hoffman J. H., Hodges, Jr., R. R. and Watson A. J. (1982) Venus was wet: a measurement of the ratio of deuterium to hydrogen. *Science* **216**, 630–633.

Drake M. J. (2005) Origin of water in the terrestrial planets. *Meteorit. Planet. Sci.* **40**, 519–527.

Dreibus G. and Wänke H. (1987) Volatiles on Earth and Mars: a comparison. *Icarus* **71**, 225–240.

Ehlers K., Grove T. L., Sisson T. W., Recca S. I. and Zervas D. A. (1992) The effect of oxygen fugacity on the partitioning of nickel and cobalt between olivine, silicate melt, and metal. *Geochim. Cosmochim. Acta* **56**, 3733–3743.

Elkins L. T. and Grove T. L. (1990) Ternary feldspar experiments and thermodynamic models. *Am. Mineral.* **75**, 544–559.

Elkins-Tanton L. T. and SeagerS. (2007) Atmospheres and oceans from initial degassing in terrestrial planets. In *Workshop on Planetary Atmospheres*, #9011 (abstr.).

Essene E. J. (1989). The current status of thermobarometry in metamorphic rocks. In *Evolution of Metamorphic Belts* (eds. S. R. Daly, R. Cliff and B. W. D. Yardley). Geol. Soc. Spec. Pap. **43**, pp. 1–44.

Evans B. W., Ghiorso M. S., Yang H. and Medenbach O. (2001) Thermodynamics of the amphiboles: anthophyllite–ferroanthophyllite and the ortho–clino phase loop. *Am. Mineral.* **86**, 640–651.

Feldman W. C. et al. (2002) Global distribution of neutrons from Mars: results from Mars Odyssey. *Science* **297**, 75–78.

Feldman W. C., Maurice S., Binder A. B., Barraclough B. L., Elphic R. C. and Lawrence D. J. (1998) Fluxes of Fast and epithermal neutrons from lunar prospector: evidence for water ice at the lunar poles. *Science* **281**, 1496–1500.

Feldman W. C., Lawrence D. J., Elphic R. C., Barraclough B. L., Maurice S., Genetay I. and Binder A. B. (2000) Polar hydrogen deposits on the Moon: new views of the moon. Part 1. *J. Geophys. Res.* **105**, 4175–4195.

Fleet M. E. and Howie R. A. (2004) *Rock-Forming Minerals. Vol. 3A: Sheet Silicates: Micas*, 2nd ed. The Geological Society, London.

Franchi I. A., Wright I. P., Sexton A. S. and Pillinger C. T. (1999) The oxygen-isotopic composition of Earth and Mars. *Meteorit. Planet. Sci.* **34**, 657–661.

Frost B. R. (1975) Contact metamorphism of serpentinite, chloritic blackwall and rodingite at Paddy-Go-Easy Pass, central Cascades, Washington. *J. Petrol.* **6**, 272–313.

Ghiorso M. S. and Sack R. O. (1995) Chemical mass transfer in magmatic processes. IV: A revised and internally consistent thermodynamic model for the interpolation and extrapolation of liquid–solid equilibria in magmatic systems at elevated temperatures and pressures. *Contrib. Mineral. Petrol.* **119**, 197–212.

Greeley R. et al. (1998) Europa: initial Galileo geological observations. *Icarus* **135**, 4–24.

Greenwood J. P., Rubin A. E. and Wasson J. T. (2000) Oxygen isotopes in R-chondrite magnetite and olivine: links between R chondrites and ordinary chondrites. *Geochim. Cosmochim. Acta* **64**, 3897–3911.

Grimm R. E. (1985) Penecontemporaneous metamorphism, fragmentation, and reassembly of ordinary chondrite parent bodies. *J. Geophys. Res.* **90**, 2022–2028.

Grossman J. N., Alexander C. M. O'D., Wang J. and Brearley A. J. (2000) Bleached chondrules: evidence for widespread aqueous processes on the parent asteroids of ordinary chondrites. *Meteorit. Planet. Sci.* **35**, 467–486.

Grossman J. N., Alexander C. M. O'D., Wang J. and Brearley A. J. (2002) Zoned chondrules in Semarkona: evidence for high- and low-temperature processing. *Meteorit. Planet. Sci.* **37**, 49–73.

Hammarstrom J. M. and Zen E. (1986) Aluminum in hornblende: an empirical igneous geobarometer. *Am. Mineral.* **71**, 1297–1313.

Hawthorne F. C. and Oberti R. (2007) Classification of the amphiboles. *Rev. Mineral. Geochem.* **67**, 55–88.

Heiken G., Vaniman D. and French B. (1991) *Lunar Sourcebook—User's Guide to the Moon*. Cambridge University Press, Cambridge, England.

Holland T. J. B. and Blundy J. (1994) Non-ideal interactions in calcic amphiboles and their bearing on amphibole–plagioclase thermometry. *Contrib. Mineral. Petrol.* **116**, 433–447.

Holland T. J. B. and Powell R. (1990) An enlarged and updated internally consistent thermodynamic data set with uncertainties and correlations: the system K_2O–Na_2O–CaO–MgO–FeO–Fe_2O_3–Al_2O_3–TiO_2–SiO_2–C–H_2–O_2. *J. Metamorph. Geol.* **8**, 89–124.

Holland T. J. B. and Powell R. (1998) An internally consistent thermodynamic data set for phases of petrological interest. *J. Metamorph. Geol.* **16**, 309–343.

Holland T. J. B. and Powell R. (2003) Activity–composition relations for phases in petrological calculations: an asymmetric multicomponent formulation. *Contrib. Mineral. Petrol.* **145**, 492–501.

Hollister L. S., Grissom G. C., Peters E. K., Stowell H. H. and Sisson V. B. (1987) Confirmation of the empirical correlation of

Al in hornblende with pressure of solidification of calc-alkaline plutons. *Am. Mineral.* **72**, 231–239.

Hutchison R., Alexander C. M. O' and Barber D. J. (1987) The Semarkona meteorite: first recorded occurrence of smectite in an ordinary chondrite, and its implications. *Geochim. Cosmochim. Acta* **51**, 1875–1882.

Imae N. and Zolensky M. (2003) Mineralogical description of PRE 95404: a Rumuruti chondrite that includes a large unequilibrated clast. *Meteorit. Planet. Sci.*, 38, #5176 (abstr.).

Jäckel A., Bischoff A., Clayton R. N. and Mayeda T. K. (1996) Dar al Gani 013—a new Saharan Rumuruti-chondrite (R3–6) with highly unequilibrated (type 3) fragments. *Lunar Planet. Sci.* **XXVII**, Lunar Planet. Inst., Houston, pp. 595–596 (abstr.).

Jarosewich E. (2006) Chemical analyses of meteorites at the Smithsonian Institution: an update. *Meteorit. Planet. Sci.* **41**, 1381–1382.

Johnson C. A. and Essene E. J. (1982) The formation of garnet in olivine-bearing metagabbros from the Adirondacks. *Contrib. Mineral. Petrol.* **81**, 240–251.

Johnson M. C. and Rutherford M. J. (1989) Experimental calibration of the aluminum-in-hornblende geobarometer with application to Long Valley Caldera (California) volcanic rocks. *Geology* **17**, 837–841.

Kallemeyn G. W., Rubin A. E. and Wasson J. T. (1996) The compositional classification of chondrites. VII: The R chondrite group. *Geochim. Cosmochim. Acta* **60**, 2243–2256.

Kasting J. F. and Pollack J. B. (1983) Loss of water from Venus. I: Hydrodynamic escape of hydrogen. *Icarus* **53**, 479–508.

Keller L. P., Messenger S., Flynn G. J., Clemett S., Wirick S. and Jacobsen C. (2004) The nature of molecular cloud material in interplanetary dust. *Geochim. Cosmochim. Acta* **68**, 2577–2589.

Kessel R., Beckett J. R. and Stolper E. M. (2007) The thermal history of equilibrated ordinary chondrites and the relationship between textural maturity and temperature. *Geochim. Cosmochim. Acta* **71**, 1855–1881.

Klima R., Pieters C., Sunshine J., Hiroi T., Bishop J., Lane M., Dyar M. D. and Treiman A. H. (2007) Coordinated spectroscopic and petrologic investigation of LAP 04840: first results of infrared, thermal and Raman spectroscopy. *Lunar Planet. Sci.* **XXXVIII**, Lunar Planet. Inst., Houston., #1710 (abstr.).

Krot A. N., Scott E. R. D. and Zolensky M. E. (1995) Mineralogical and chemical modification of components in CV3 chondrites: Nebular or asteroidal processing? *Meteoritics* **30**, 748–775.

Krot A. N., Petaev M. I., Scott E. R. D., Choi B.-G., Zolensky M. E. and Kiel K. (1998) Progressive alteration in CV3 chondrites: more evidence for asteroidal alteration. *Meteorit. Planet. Sci.* **33**, 1065–1085.

Leake B. E. et al. (1997) Nomenclature of amphiboles: report of the subcommittee on amphiboles of the International Mineralogical Association Commission on New Minerals and Mineral Names. *Eur. J. Mineral.* **9**, 623–651.

Lentz R. C. F., McSween, Jr., H. Y., Ryan J. and Riciputi L. R. (2001) Water in Martian magmas: clues from light lithophile elements in shergottite and nakhlite pyroxenes. *Geochim. Cosmochim. Acta* **65**, 4551–4565.

Liermann H. P. and Ganguly J. (2003) Fe^{2+}–Mg fractionation between orthopyroxene and spinel: experimental calibration in the system FeO–MgO–Al_2O_3–Cr_2O_3–SiO_2, and applications. *Contrib. Mineral. Petrol.* **145**, 217–227.

Liermann H. P. and Ganguly J. (2007) Erratum: Fe^{2+}–Mg fractionation between orthopyroxene and spinel: experimental calibration in the system FeO–MgO–Al_2O_3–Cr_2O_3–SiO_2, and applications. *Contrib. Mineral. Petrol.* **154**, 491.

Lindsley D. H. and Anderson D. J. (1983) A two-pyroxene thermometer. *J. Geophys. Res.* **88**, A887–A906.

Lin L.-H., Slater G. F., Sherwood Lollar B., Lacrampe-Couloume G. and Onstott T. C. (2005) The yield and isotopic composition of radiolytic H_2, a potential energy source for the deep subsurface biosphere. *Geochim. Cosmochim. Acta* **69**, 893–903.

MacPherson G. J., Hashimoto A. and Grossman L. (1985) Accretionary rims on inclusions in the Allende Meteorite. *Geochim. Cosmochim. Acta* **49**, 2267–2279.

Malin M. C. and Edgett K. S. (2000) Evidence for recent groundwater seepage and surface runoff on Mars. *Science* **288**, 2330–2335.

McGuire A. V., Dyar M. D. and Nielson J. E. (1991) Metasomatic oxidation of upper mantle peridotite. *Contrib. Mineral. Petrol.* **109**, 252–264.

McKeegan K. D. and Leshin L. A. (2001) Stable isotope variations in extraterrestrial materials. In *Stable Isotope Geochemistry*, vol. 43 (eds. J. W. Valley and D. R. Cole). Mineralogical Society of America, Washington, DC, pp. 279–318.

McNaughton N. J., Fallick A. E. and Pillinger C. T. (1982) Deuterium enrichments in type 3 ordinary chondrites. *J. Geophys. Res.* **87**, A297–A302.

McSween, Jr., H. Y. (1979) Alteration in CM carbonaceous chondrites inferred from modal and chemical variations in matrix. *Geochim. Cosmochim. Acta* **43**, 1761–1770.

McSween, Jr., H. Y. and Patchen A. D. (1989) Pyroxene thermobarometry in LL-group chondrites and implications for parent body metamorphism. *Meteoritics* **24**, 219–226.

McSween, Jr., H. Y., Ghosh A., Grimm R. E., Wilson L. and Young E. D. (2002) Thermal evolution models of asteroids. In *Meteorites and the Early Solar System*, vol. II (eds. D. S. Lauretta and H. Y. McSween). University of Arizona Press, Tucson, pp. 559–571.

Melosh H. J. (1989) *Impact Cratering: A Geologic Process*. Oxford University Press, New York.

Messenger S. (2002) Deuterium enrichments in interplanetary dust. *Planet. Space Sci.* **50**, 1221–1225.

Metzler K., Bischoff A. and Stöffler D. (1991) Accretionary dust mantles in CM chondrites: evidence for solar nebula processes. *Geochim. Cosmochim. Acta* **56**, 2873–2897.

Mikouchi T., Ota K., Makishima J., Monkawa A. and Sugiyama K. (2007) Mineralogy and crystallography of LAP 04840: implications for metamorphism at depth in the R chondrite parent body. *Lunar Planet. Sci.* **XXXVIII**, Lunar Planet. Inst., Houston. #1928 (abstr.).

Mumma M. J., Weissman P. R. and Stern S. A. (1993) Comets and the origin of the Solar System: reading the Rosetta Stone. In *Protostars and Planets*, vol. III (eds. E. H. Levy and J. I. Lunine). University of Arizona Press, Tucson, pp. 1177–1252.

Munoz J. L. (1984) F–OH and Cl–OH exchange in micas with applications to hydrothermal deposits. In *Micas*, vol. 13 (ed. S. W. Bailey). Mineralogical Society of America, Washington, D.C., pp. 469–493.

Munoz J. L. (1992) Calculation of HF and HCl fugacities from biotite compositions: revised equations. *Geol. Soc. Am., Abstr. Prog.* **24**, A221.

Munoz J. L. and Ludington S. D. (1974) Fluorine-hydroxyl exchange in biotite. *Am. J. Sci.* **274**, 396–415.

Nakamura T. (2005) Post-hydration thermal metamorphism of carbonaceous chondrites. *J. Mineral. Petrol. Sci.* **100**, 260–272.

Nakamura T., Tomeoka K. and Takeda H. (1993) Mineralogy and petrology of the CK chondrites Yamato-82104, -693 and a Carlisle Lakes-type chondrite Yamato-82002. In *Proc. NIPR Sym. Ant. Met*, vol. 6, pp. 171–185.

Naumov M. V. (2005) Principal features of impact-generated hydrothermal circulation systems: mineralogical and geochemical evidence. *Geofluids* **5**, 165–184.

Ohtani E. (2005) Water in the mantle. *Elements* **1**, 25–30.

O'Neill H. St. C. and Wall V. J. (1987) The olivine–orthopyroxene–spinel oxygen geobarometer, the nickel precipitation curve, and the oxygen fugacity of the Earth's upper mantle. *J. Petrol.* **28**, 1169–1191.

Porco C. C. et al. (2006) Cassini observes the south pole of Enceladus. *Science* **311**, 1393–1401.

Powell R. and Holland T. J. B. (1988) An internally consistent dataset with uncertainties and correlations. 3. Applications to geobarometry, worked examples and a computer program. *J. Metamorph. Geol.* **6**, 173–204.

Powell R. and Holland T. J. B. (2001) *Course Notes for THERMOCALC Workshop 2001: Calculating Metamorphic Phase Equilibria* (CD-ROM).

Remusat L., Palhol F., Robert F., Derenne S. and France-Lanord C. (2006) Enrichment of deuterium in insoluble organic matter from primitive meteorites: a solar system origin? *Earth Planet. Sci. Lett.* **243**, 15–25.

Richardson D. C., Leinhardt Z. M., Melosh H. J., Bottke, Jr., W. F. and Asphaug E. (2002) Gravitational aggregates: evidence and evolution. In *Asteroids*, vol. III (eds. , Jr.W. F. Bottke, A. Cellino, P. Paolicchi and R. P. Binzel). University of Arizona Press, Tucson, pp. 501–515.

Righter K. and Neff K. E. (2007) Temperature and oxygen fugacity constraints on CK and R chondrite, and implications for water and oxidation in the early solar system. *Pol. Sci.* **1**, 25–44.

Robert F. (2002) Water and organic matter D/H ratios in the solar system: a record of an early irradiation of the nebula? *Planet. Space Sci.* **50**, 1227–1234.

Robert F. and Epstein S. (1982) The concentration and isotopic composition of hydrogen, carbon and nitrogen in carbonaceous meteorites. *Geochim. Cosmochim. Acta* **46**, 81–95.

Robie R. A., Hemingway B. S. and Fischer J. R. (1978) *Thermodynamic Properties of Minerals and Related Substances at 298.15 K and 1 bar (10^5 Pascals) Pressure and at Higher Temperatures.* U.S. Geol. Surv. Bull. 1452, U.S. Govt. Printing Office.

Rolston J. H., den Hartog J. and Butler J. P. (1976) The deuterium isotope separation factor between hydrogen and liquid water. *J. Phys. Chem.* **80**, 1064–1067.

Rubin A. E. and Kallemeyn G. W. (1989) Carlisle Lakes and Allan Hills 85151: members of a new chondrite grouplet. *Geochim. Cosmochim. Acta* **53**, 3035–3044.

Rubin A. E. and Kallemeyn G. W. (1994) Pecora Escarpment 91002: a member of the new Rumuruti (R) chondrite group. *Meteoritics* **29**, 255–264.

Rubin A. E., Trigo-Rodriguez J. M., Huber H. and Wasson J. T. (2007) Progressive aqueous alteration of CM carbonaceous chondrites. *Geochim. Cosmochim. Acta* **71**, 2361–2382.

Rumble D., Miller M. F., Franchi I. A. and Greenwood R. C. (2007) Oxygen three-isotope fractionation lines in terrestrial silicate minerals: an inter-laboratory comparison of hydrothermal quartz and eclogitic garnet. *Geochim. Cosmochim. Acta* **71**, 3592–3600.

Saal A. E., Hauri E. H., LoCascio M., Van Orman J., Rutherford M. J. and Cooper R. F. (2007) The volatile contents (CO_2, H_2O, F, S, Cl) of the lunar picritic glasses. In *Workshop on Water in Planetary Basalts*. Lunar Planet. Inst. Houston. #2009 (abstr.).

Sack R. O. and Ghiorso M. S. (1991) Chromian spinels as petrogenetic indicators: thermodynamics and petrological applications. *Am. Mineral.* **76**, 827–847.

Satterwhite C. and Righter K. (2006). *Antarctic Meteorit. Newslett.* **29**, 24.

Schmidt M. W. (1992) Amphibole composition in tonalite as a function of pressure: an experimental calibration of the Al-in-hornblende barometer. *Contrib. Mineral. Petrol.* **110**, 304–310.

Schulze H., Bischoff A., Palme H., Spettel B., Dreibus G. and Otto J. (1994) Mineralogy and chemistry of Rumuruti: the first meteorite fall of the new R chondrite group. *Meteoritics* **29**, 275–286.

Scott E. R. D. and Wilson L. (2005) Meteoritic and other constraints on the internal structure and impact history of small asteroids. *Icarus* **174**, 46–53.

Shedlock R. J. and Essene E. J. (1979) Mineralogy and petrology of a tactite near Helena, Montana. *J. Petrol.* **20**, 71–97.

Sisson V. B. (1987) Halogen geochemistry as an indicator of metamorphic fluid interaction with the Ponder Pluton, Coast Plutonic Complex, British Columbia, Canada. *Contrib. Mineral. Petrol.* **95**, 123–131.

Slade M. A., Butler B. J. and Muhleman D. O. (1992) Mercury radar imaging: evidence for polar ice. *Science* **258**, 635–640.

Slater-Reynolds V. and McSween, Jr., H. Y. (2005) Peak metamorphic temperatures in type 6 ordinary chondrites: an evaluation of pyroxene and plagioclase geothermometry. *Meteorit. Planet. Sci.* **40**, 745–754.

Spear F. S. (1981) An experimental study of hornblende stability and compositional variability in amphibolite. *Am. J. Sci.* **281**, 697–734.

Spear F. S. (1993) *Metamorphic Phase Equilibria and Pressure–Temperature–Time Paths*. Mineralogical Society of America, Washington, DC.

Squyres S. W. et al. (2006) Two years at Meridiani Planum: results from the Opportunity Rover. *Science* **313**, 1403–1407.

Stoffler D., Keil K. and Scott E. R. D. (1991) Shock metamorphism of ordinary chondrites. *Geochim. Cosmochim. Acta* **55**, 3845–3867.

Tischendorf G., Foerster H. J., Gottesmann B. and Rieder M. (2007) True and brittle micas: composition and solid–solution series. *Mineral. Mag.* **71**, 285–320.

Tomeoka K. and Busek P. R. (1985) Hydrated interplanetary dust particle linked with carbonaceous chondrites? *Nature* **314**, 338–340.

Tonui E., Zolensky M. and Lipschutz M. (2002) Petrography, mineralogy, and trace element chemistry of Yamato-86029, Yamato-793321, and Lewis Cliffs 85332: aqueous alteration and heating events. *Antarctic Meteorit. Res.* **15**, 38–58.

Toulmin, III, P. and Barton, Jr., P. B. (1964) A thermodynamic study of pyrite and pyrrhotite. *Geochim. Cosmochim. Acta* **28**, 641–671.

Treiman A. H. (2005) The nakhlite Martian meteorites: augite-rich igneous rock from Mars. *Chem. Erde* **65**, 203–270.

Treiman A. H., Musselwhite D. S., Herd C. D. K. and Shearer, , C. K. (2006) Light lithophile elements in pyroxenes of NWA817 and other Martian meteorites: implications for water in Martian magmas. *Geochim. Cosmochim. Acta* **70**, 2919–2934.

van Schmus W. R. and Wood J. A. (1967) A chemical–petrologic classification for the chondritic meteorites. *Geochim. Cosmochim. Acta* **31**, 747–765.

Vilas F. and Gaffey M. J. (1989) Phyllosilicate absorption features in main-belt and outer-belt asteroids from reflectance spectroscopy. *Science* **246**, 790–792.

Vilas F., Hatch E. C., Larson S. M., Sawyer S. R. and Gaffey M. J. (1993) Ferric iron in primitive asteroids: a 0.43 mm absorption feature. *Icarus* **102**, 225–231.

Vilas F., Jarvis K. S. and Gaffey M. J. (1994) Iron alteration minerals in the visible and near-infrared spectra of low-albedo asteroids. *Icarus* **109**, 274–283.

von Seckendorf V. and O'Neill H. St. C. (1993) An experimental study of Fe–Mg partitioning between olivine and orthopyroxene at 1173, 1273 and 1423 K at 1.6 GPa. *Contrib. Mineral. Petrol.* **113**, 196–207.

Watson L. L., Hutcheon I. D., Epstein S. and Stolper E. M. (1994) Water on Mars: clues from deuterium/hydrogen and water contents of hydrous phases in SNC meteorites. *Science* **265**, 86–90.

Weber D., Schultz L., Weber H. W., Clayton R. N., Mayeda T. K. and Bischoff A. (1997) Hammadah al Hamra 119: a new, unbrecciated Saharan Rumuruti chondrite. *Lunar Planet. Sci. XXVIII*, Lunar Planet. Inst., Houston, pp. 511–512 (abstr.).

Weisberg M. K. and Huber H. (2007) The Grosvenor Mountains 95577 CR1 chondrite and hydration of the CR parent body. *Meteorit. Planet. Sci.* **42**, 1495–1503.

Weisberg M. K. and Prinz M. (2000) The Grosvenor Mountains 95577 CR1 chondrite and hydration of the CR chondrites. *Meteorit. Planet. Sci.* **35**, A168 (abstr.).

Weisberg M. K., Prinz M., Clayton R. N. and Mayeda T. K. (1993) The CR (Renazzo-type) carbonaceous chondrite group and its implications. *Geochim. Cosmochim. Acta* **57**, 1567–1586.

Wlotzka F. (2005) Cr spinel and chromite as petrogenetic indicators in ordinary chondrites: equilibration temperatures of petrologic types 3.7 to 6. *Meteorit. Planet. Sci.* **40**, 1673–1702.

Wood B. J. (1991) Oxygen barometry of spinel peridotites. In *Oxide Minerals: Petrologic and Magnetic Significance*, vol. 25 (eds. D. H. Lindsley and P. H. Ribbe). Mineralogical Society of America, Washington, DC, pp. 417–432.

Yang J. and Epstein S. (1984) Relic interstellar grains in Murchison meteorite. *Nature* **311**, 544–547.

Zhu C. and Sverjensky D. A. (1992) F–Cl–OH partitioning between biotite and apatite. *Geochim. Cosmochim. Acta* **56**, 3435–3467.

Associate editor: Sara S. Russell